10 Noise and Vibration from Railway Vehicles

David Thompson and Chris Jones

CONTENTS

I. INTRODUCTION

A. The Importance of Noise and Vibration

Environmental noise is an issue that has seen increased awareness in recent years. Within the European Union (E.U.) it is estimated[1] that 20% of the population live in areas with unacceptable noise levels.[a] Noise is often cited as a major factor contributing to people's dissatisfaction with their environment. While this noise exposure is usually due mainly to road traffic, trains also contribute significantly in the vicinity of railway lines. Road vehicles and aircraft have long been the subject of legislation that limits their noise emissions. The E.U. has therefore recently introduced noise limits for new rail vehicles. These have been implemented as part of the Technical Specifications for Interoperability (TSIs), which initially cover high speed trains[2] and are being extended to include conventional trains. They state noise limits for new trains under both static and running conditions.

By contrast with exterior noise, the noise inside a vehicle (road or rail) is not generally the subject of legislation, apart from the noise inside the driver's cab. For road vehicles, noise is actually used as a major factor to distinguish vehicles from their competitors and to attract people to buy a particular vehicle. As rail vehicles are for mass use, interior noise is subject instead to specifications from the purchasing organisation. These are usually limited to ensuring that problems are eliminated and that the vehicles are fit for their purpose.

Railway operations also generate vibrations that are transmitted through the ground into neighbouring properties. These can lead either to feelable vibration (in the range 4 to 80 Hz) or to low frequency rumbling noise (30 to 250 Hz). Vibrations are also transmitted into the vehicle itself, affecting passenger comfort.

B. Basics of Acoustics

The field of acoustics is too large to cover in detail here. This chapter therefore gives only a very brief overview of some basic quantities. The interested reader is referred to textbooks on the subject for further details.[3,4]

Sound consists of audible fluctuations in pressure, usually of the air. These propagate through the air as waves with a wave speed, denoted by c_0, of about 340 m/sec in air at 20°C.

[a] This is expressed as levels above 65 dB, L_{Aeq}. The L_{Aeq} is the A-weighted equivalent noise level averaged over a period of, for example, a day (or night).

Simultaneously, fluctuations in air density and particle motion also occur. To express the magnitude of a sound, the root mean square (rms) sound pressure is usually used:

$$p_{\text{rms}} = \left(\frac{1}{T} \int_{t_1}^{t_1+T} p^2(t) \mathrm{d}t \right)^{1/2} \tag{10.1}$$

where $p(t)$ is the instantaneous sound pressure and T is the averaging time. Much use is made of frequency analysis, whereby sound signals are decomposed into their frequency content (e.g., using Fourier analysis). The normal ear is sensitive to sound in the frequency range 20 to 20,000 Hz (the upper limit reduces with age and with noise exposure) and to a large range of amplitudes (around six orders of magnitude). Owing to these large ranges, and to mimic the way the ear responds to sound, logarithmic scales are generally used to present acoustic data. Thus amplitudes are expressed in decibels. The *sound pressure level* (NB level implies decibels) is defined as:

$$L_p = 10 \log_{10} \left(\frac{p_{\text{rms}}^2}{p_{\text{ref}}^2} \right) = 20 \log_{10} \left(\frac{p_{\text{rms}}}{p_{\text{ref}}} \right) \tag{10.2}$$

where the reference pressure p_{ref} is usually 2×10^{-5} Pa. Frequencies (expressed in Hz) are also generally plotted on logarithmic scales, with *one-third octave bands* being a common form of presentation. The frequency range is divided into bands that are of equal width on a logarithmic scale. The centre frequencies of each band can be given by $10^{(N/10)}$ where N is the band number, although by convention they are rounded to particular values. Bands 13 to 43 cover the audible range.

The total sound emitted by a source is given by its power, W, which in decibel form is given as the *sound power level*:

$$L_W = 10 \log_{10} \left(\frac{W}{W_{\text{ref}}} \right) \tag{10.3}$$

where the reference power, W_{ref}, is usually 10^{-12} W. The power is generally proportional to the square of the sound pressure, so that a 1-dB increase in sound power level leads to a 1-dB increase in sound pressure level at a given location. However, sound pressure also depends on the location, usually reducing as the receiver becomes further from the source. For a compact point source this reduction is 6 dB per doubling of distance, while for a line source it is 3 dB per doubling. Other quantities can also be expressed in decibels following the pattern of Equation 10.2 and Equation 10.3.

It should be realised that sound generation is often a very inefficient process. The *proportion* of the mechanical power of a typical machine that is converted into sound is often in the range 10^{-7} to 10^{-5}. Sound is generated by various mechanisms, but the two main ones are:

- *Structural vibrations* — the vibration of a structure causes the air around it to vibrate and transmit sound, e.g., a drum, a loudspeaker, wheels and rails.
- *Aerodynamic fluctuations* — wind, particularly turbulence and flow over solid objects, also produces sound, e.g., jet noise, turbulent boundary layer noise, exhaust noise, fan noise.

It can be pointed out that *noise* differs from *sound* in that noise is unwanted sound. While the acceptability of sound levels and signal content varies greatly between individuals, it is important to include some approximation to the way the ear weights different sounds. Several weighting curves have been devised, but the A-weighting (Figure 10.1) is the most commonly used. This approximates the inverse of the equal loudness curve at about 40 dB. As the ear is most

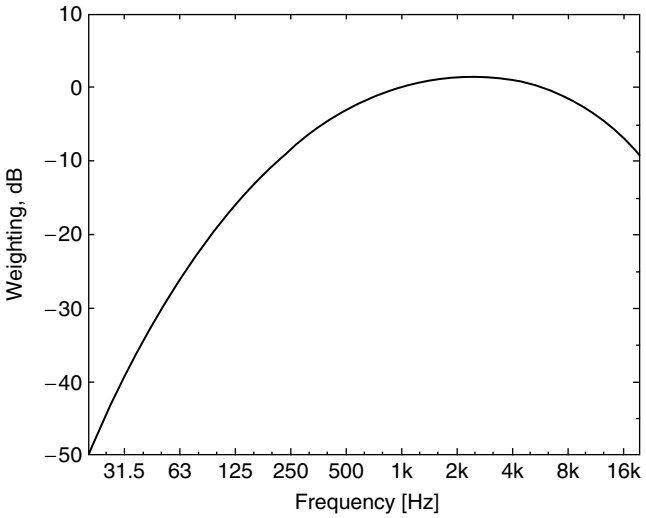

FIGURE 10.1 The A-weighting curve.

sensitive around 1 to 5 kHz and much less sensitive at low and high frequencies, more prominence is given to this central part of the spectrum. The overall sound level is often quoted as an A-weighted value, meaning that this weighting curve is applied to the spectrum before calculating the total.

Another overall measure of the magnitude of a sound is the *loudness*. Strictly, this is a subjective quantity, but there are ways of calculating a loudness value from a one-third octave band spectrum.[5] However, this is less commonly used than the A-weighted decibel. It should be borne in mind that an increase of 10 dB is perceived as a doubling of loudness, while a change of less than 3 dB is normally imperceptible.

C. Sources of Railway Noise and Vibration

In the case of railway noise, both of the above types of mechanism apply. Aerodynamic noise is important for high-speed operation and is generated by unsteady airflow, particularly over the nose, intercarriage joints, bogie regions, louvres, and roof-mounted equipment such as pantographs. However, mechanical sources of noise are also present on a train and these dominate the overall noise for speeds up to about 300 km/h.

The most important mechanical noise source from a train is generated at the wheel–rail contact. Rolling noise is caused by vibrations of the wheel and track structures, induced at the wheel–rail contact point by vertical irregularities in the wheel and rail surfaces. A similar mechanism leads to noise due to discontinuities in the wheel or rail surface (impact noise). Squeal noise occurs in sharp curves and is induced by unsteady friction forces at the wheel–rail contact. Finally, ground-borne vibration and noise are caused by track and wheel irregularities and by the movement of the set of axle loads along the track. Each of these sources of noise and vibration are discussed in turn in the following sections.

II. ROLLING NOISE

A. Mechanism of Rolling Noise Generation

As indicated above, rolling noise is usually the dominant source of noise from moving trains at speeds below about 300 km/h. It can be attributed to components radiated by vibration of both

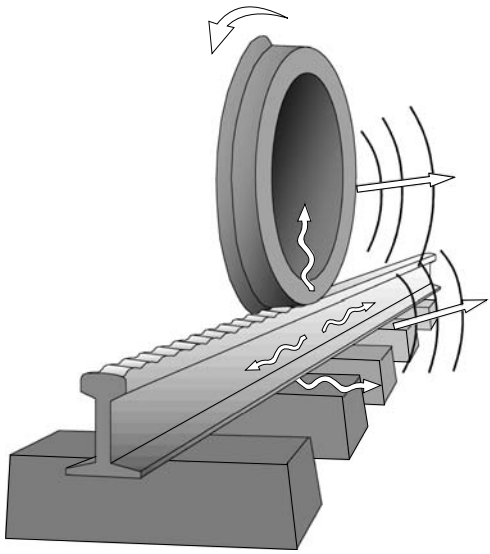

FIGURE 10.2 Schematic view of how rolling noise is generated at the wheel–rail interface.

the wheels and track. This vibration is caused by the combined surface roughness at their interface, as shown in Figure 10.2.

The relative importance of the components of sound radiation from the wheel and track depends on their respective designs as well as on the train speed and the wavelength content of the surface roughness. In most cases both sources (wheel and track) are significant. As the noise radiation depends on the roughness of both the wheel and track, it is possible that a rough wheel causes a high noise level that is mainly radiated by the track vibration or vice versa. It is therefore difficult to assign noise contributions solely to the vehicle or infrastructure.

B. Surface Roughness

Irregularities with wavelengths between about 5 and 500 mm cause the vibrations of relevance to noise. When a wavelength λ, in m, is traversed at a speed ν, in m/s, the associated frequency generated (in Hz) is given by:

$$f = \frac{\nu}{\lambda} \tag{10.4}$$

The corresponding amplitudes range from over 50 μm at long wavelengths to much less than 1 μm at short wavelengths. Typical wheel roughness spectra are shown in Figure 10.3. These are given in decibels relative to 1 μm (using a definition equivalent to Equation 10.2), expressed in one-third octave bands over wavelength.

In the TSIs,[2] a standard is included for the roughness of a test track that is used to measure vehicles. The roughness should be less than a specified spectrum, shown in Figure 10.4. This represents good quality track. The purpose of this is to ensure that variations in rail roughness from one site to another do not significantly affect the measurement, as the wheel roughness will usually be at least as large as the rail roughness (see Figure 10.3).

The wheel–rail contact does not occur at a point but over a small area. The *contact patch* is typically 10- to 15-mm long and a similar width. When roughness wavelengths are short compared with the contact patch length, their effect on the wheel–rail system is attenuated. This effect is

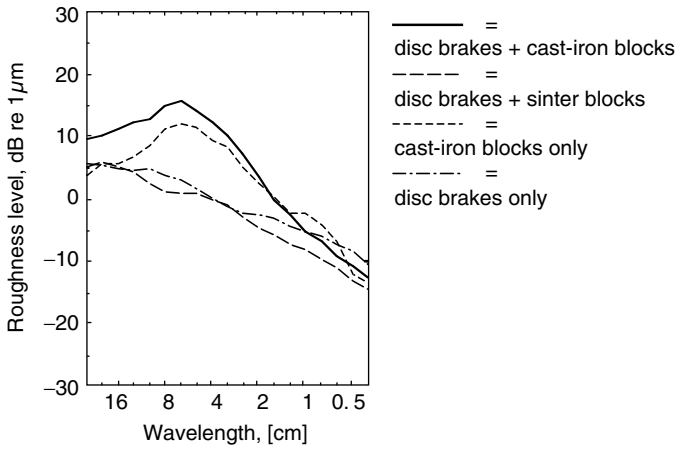

FIGURE 10.3 Typical wheel roughness spectra.[6]

known as the contact filter. This is significant from about 1 to 1.5 kHz for a speed of 160 km/h, and at lower frequencies for lower speeds.

In early analytical models for this effect,[7] the extent of the correlation of the roughness across the width of the contact had to be assumed since very detailed roughness data were not available. Figure 10.5a shows results from this model for a contact patch length of 11 mm. The parameter α determines the extent of correlation across the width that is assumed. More recently, Remington has developed a numerical discrete point reacting spring (DPRS) model.[8] This model is intended to be used with roughness measurements obtained on multiple parallel lines a few millimetres apart. Figure 10.5b from Ref. 9, shows results obtained using a series of such measurements in combination with the DPRS model. This confirms the validity of the analytical model at low frequencies but indicates that the filtering effect is less severe at high frequencies than the analytical model suggests.

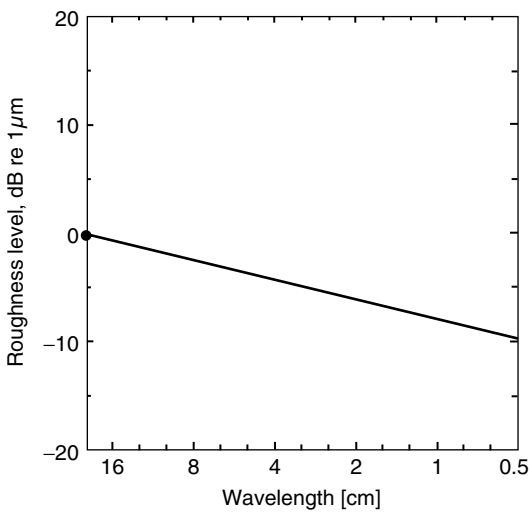

FIGURE 10.4 Maximum roughness allowed for vehicle noise measurements according to high-speed train TSI.[2]

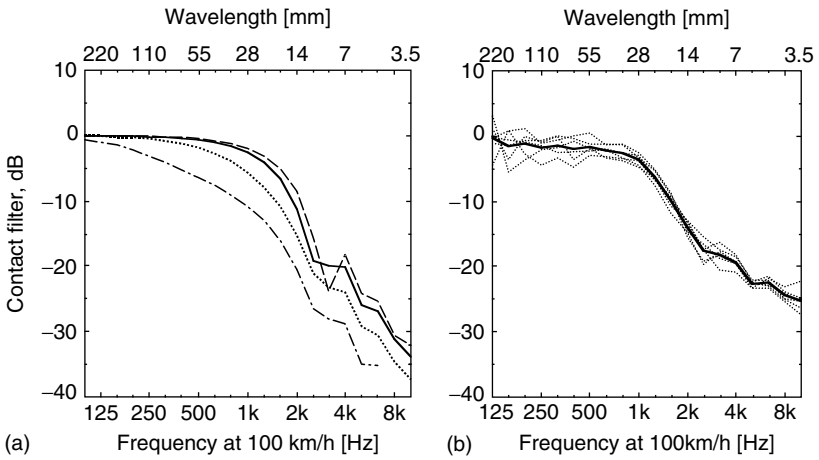

FIGURE 10.5 Contact filter due to contact patch of semiaxis length 5.7 mm. (a) Analytical model: — $\alpha = 1$,– – – $\alpha = 0.1$, … $\alpha = 3$,–. –. – $\alpha = 10$. (b) Numerical DPRS model for data from three cast-iron block-braked wheels, one disc-braked wheel, and two sinter block braked wheels. — Mean of six wheels.[9] *Source*: From Thompson, D. J., *J. Sound Vib.*, 267, 523–535, 2003, Elsevier. With permission.

C. Wheel Dynamics

A railway wheel is a lightly damped resonant structure, which when struck rings like a bell, a structure which it strongly resembles. As with any structure, the frequencies at which it vibrates freely are called its "resonance" or "natural" frequencies and the associated vibration pattern is called the mode shape.

Wheels are usually axisymmetric (although the web is sometimes not). Their normal modes of vibration can therefore be described in terms of the number of diametral node lines — lines at which the vibration pattern has a zero. A flat disc, to which a wheel can be approximated, has out-of-plane modes that can be described by the number of nodal diameters, n, and the number of nodal circles, m. A perfectly flat disc also has in-plane radial modes with n nodal diameters and circumferential modes with n nodal diameters. In-plane modes with nodal circles occur for railway wheels above 6 kHz.

A railway wheel differs from a flat disc, having a thick tyre region at the perimeter and a thick hub at the centre connecting the wheel to the axle. A railway wheel is also not symmetric about a plane perpendicular to its axis. The tyre region is asymmetric due to the flange, and the web is usually also asymmetric, at least on wheels designed for tread braking, the curved web being designed to allow for thermal expansion. An important consequence of this asymmetry is that radial and out-of-plane (axial) modes are coupled.

The finite element method can be used quite effectively to calculate the natural frequencies and mode shapes of a railway wheel. Figure 10.6 shows an example of results for a UIC 920-mm freight wheel.[10]

The cross-section through the wheel is shown, along with an exaggerated form of the deformed shape in each mode of vibration. Each column contains modes of a particular number of nodal diameters, n. The first row contains axial modes with no nodal circle. These have their largest out-of-plane vibration at the running surface of the wheel. These modes are usually excited in curve squeal (see Section V below) but are not excited significantly in rolling noise. The second and third rows contain one-nodal-circle axial modes and radial modes. Owing to the asymmetry of the wheel cross-section, and their proximity in frequency, these two sets of modes are strongly coupled, that is, both contain axial *and* radial motion. It is these modes that are most strongly excited by roughness during rolling on straight track, due to their radial component at the wheel–rail contact point.

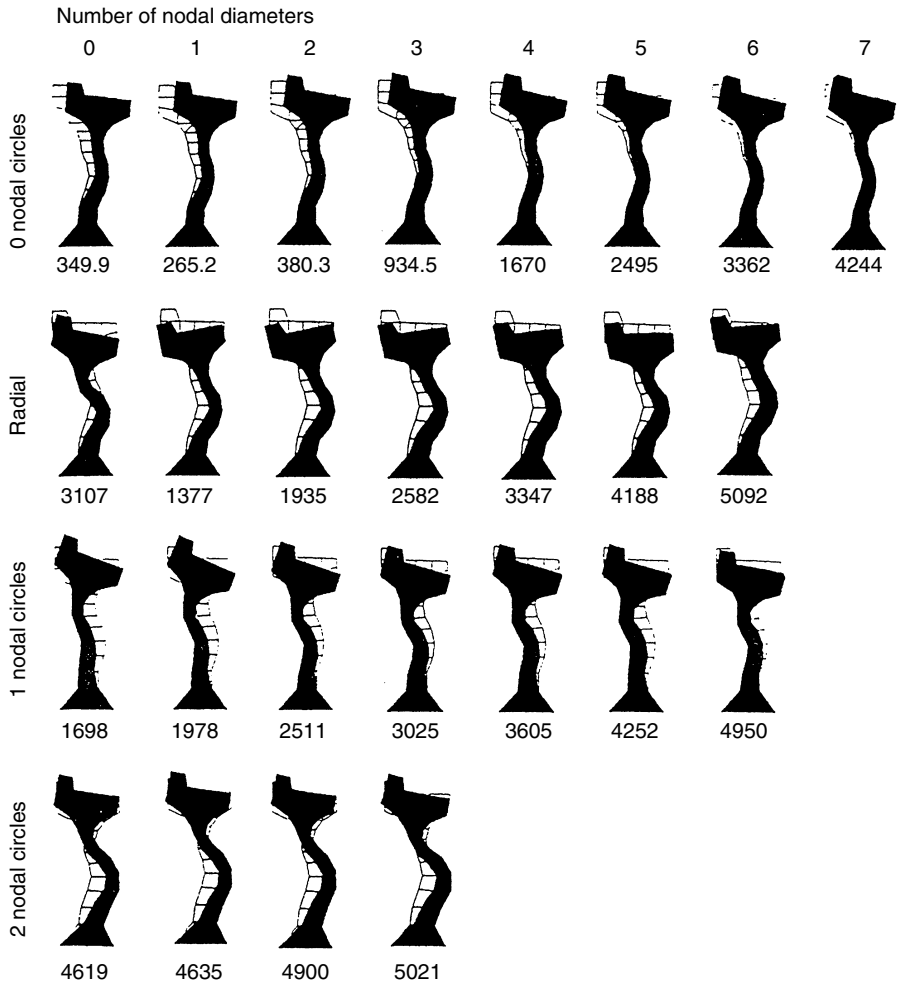

FIGURE 10.6 Modes of vibration and natural frequencies (in Hz) of UIC 920-mm freight wheel calculated using finite elements.[10] *Source*: From Thompson, D. J., *J. Sound Vib.*, 231, 519–536, 2000, Elsevier. With permission.

The modes shown in Figure 10.6 are of the wheel alone, constrained rigidly at the inner edge of its hub. The first column of modes, $n = 0$, are in practice coupled to extensional motion in the axle, and the second set, $n = 1$, are coupled to bending motion in the axle. As a result of this coupling with the axle, which is constrained by the roller bearings within the axle boxes, these sets of modes experience greater damping than the modes with $n \geq 2$. The latter do not involve deformation of the axle and therefore are damped only by material losses; their modal damping ratios are typically about 10^{-4}.

In order to couple the wheel to the track in a theoretical model, the frequency response functions of the wheel at the interface point are required. These may be expressed in terms of receptance, the vibration displacement due to a unit force as a function of frequency. Alternatively, mobility, the velocity divided by force, or accelerance, the acceleration divided by force, can be used.

Such frequency response functions of a structure can be constructed from a modal summation. For each mode, the natural frequency f_{mn} is written as a circular frequency $\omega_{mn} = 2\pi f_{mn}$.

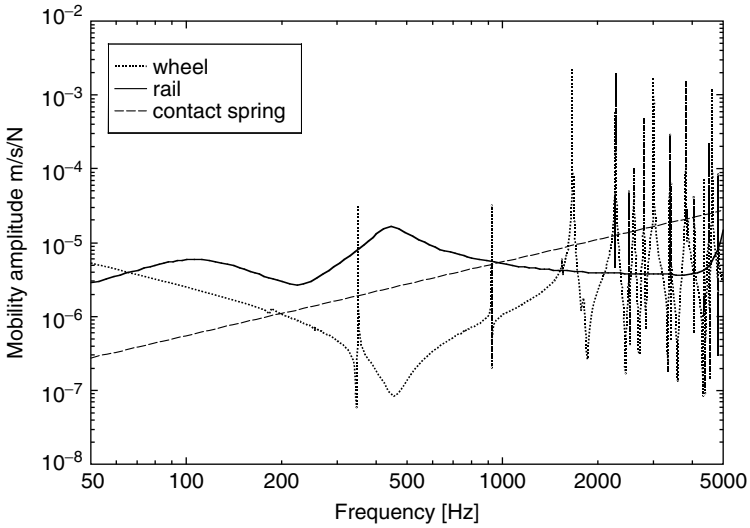

FIGURE 10.7 Vertical mobilities of the wheel–rail system. Radial mobility of UIC 920-mm freight wheel, vertical mobility of track with moderately soft pads and contact spring mobility.

Then the response at circular frequency ω, in the form of a receptance α_{jk}^{W} is:

$$\alpha_{jk}^{W} = \sum_{n,m} \frac{\psi_{mnj}\psi_{mnk}}{m_{mn}(\omega_{mn}^2 - \omega^2 + 2i\zeta_{mn}\omega\omega_{mn})} \tag{10.5}$$

where ψ_{mnj} is the mode shape amplitude of mode m,n at the response position,
ψ_{mnk} is the mode shape amplitude of mode m,n at the force position,
m_{mn} is the modal mass of mode m,n, a normalisation factor for the mode shape amplitude,
ζ_{mn} is the modal damping ratio of mode m,n,
i is the square root of -1.

Figure 10.7 shows the radial point mobility of a wheelset calculated using the normal modes from a finite element model as shown in Figure 10.6. This is based on Equation 10.5 multiplied by $i\omega$ to convert from receptance to mobility. At low frequencies the mobility is inversely proportional to frequency, corresponding to mass-like behaviour. Around 500 Hz an antiresonance trough appears and above this frequency the curve rises in stiffness-like behaviour until a series of sharp resonance peaks are reached at approximately 2 kHz. These peaks are the axial one-nodal-circle and radial sets of modes, identified in Figure 10.6.

D. Track Dynamics

The dynamic behaviour of track is described in detail in Chapter 6. A typical track mobility is also shown in Figure 10.7. This is predicted using a model based on a continuously supported rail, which neglects the effects of the periodic support. A broad peak at around 100 Hz corresponds to the whole track vibrating on the ballast. At the second peak, at approximately 500 Hz, the rail vibrates on the rail pad stiffness. The frequency of this peak depends on the rail pad stiffness. Above this frequency, bending waves propagate in the rail and can be transmitted over quite large distances.

The degree to which these waves are attenuated, mainly due to the damping effect of the pads and fasteners, affects the noise radiation from the rail. Figure 10.8 shows measured decay rates of vertical vibration for three different rail pads installed in the same track. The results for the middle

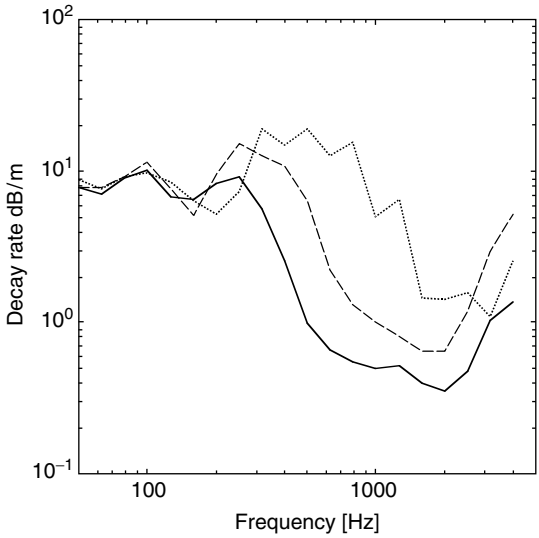

FIGURE 10.8 Measured decay rate of vertical vibration along the track for three different rail pads: — 140, – – – 300, and ··· 1000 MN/m.

value of pad stiffness corresponds to the mobility in Figure 10.7. The vertical bending waves are strongly attenuated in a region between 300 and 800 Hz which depends on the pad stiffness. This peak in the decay rate corresponds to the region between the two resonance peaks in Figure 10.7. Here, the sleeper mass vibrates between the pad and ballast springs and acts as a dynamic absorber to attenuate the propagation of waves in the track. The attenuation of lateral waves is generally smaller than for the vertical direction.

E. Wheel–Rail Interaction

The wheel and rail are coupled dynamically at their point of contact. Between them local elastic deflection occurs to form the contact patch, which can be represented as a contact spring. Although this spring is nonlinear (see Chapter 4), for small dynamic deflections it can be approximated by a linearised stiffness, k_H.[11] This is shown as a mobility ($= i\omega/k_H$) in Figure 10.7.

The coupled wheel–rail system is excited by the roughness, which forms a relative displacement input (see Figure 10.9). Here, the motion of the wheel is ignored and the system is replaced by one in which the wheel is static and the roughness is pulled between the wheel and rail (moving irregularity model). Considering only coupling in the vertical direction, from equilibrium of forces and compatibility of displacements, the vibration amplitude of the wheel (u_W) and rail (u_R) at a particular frequency can be written as:

$$u_W = \frac{\alpha_W r}{\alpha_W + \alpha_R + \alpha_C}; \qquad u_R = \frac{-\alpha_R r}{\alpha_W + \alpha_R + \alpha_C} \tag{10.6}$$

where r is the roughness amplitude and α_{W}, α_{R}, α_{C} are the vertical receptances of the wheel, rail, and contact spring, respectively. Clearly, where the rail receptance has a much larger magnitude than that of the wheel or contact spring, $u_R \approx -r$, that is, the rail is pushed down at the amplitude of the roughness. From Figure 10.7, this can be expected between approximately 100 and 1000 Hz. Changing the rail receptance in this frequency region has little effect on the rail vibration at the contact point (although the changes may affect the decay rates).

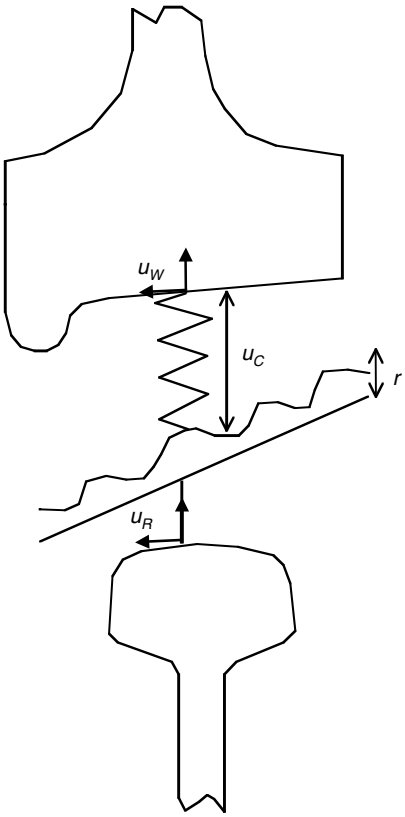

FIGURE 10.9 The wheel–rail contact showing excitation by roughness of amplitude r.

In practice, coupling also exists in other directions as well as the vertical, notably the lateral direction. This modifies Equation 10.6 to yield a matrix equation, but the principle remains the same.

F. Noise Radiation

The vibrations of the wheel, rail, and sleepers all produce noise. In general, the sound power W_{rad} radiated by a vibrating surface of area S can be expressed as:

$$W_{\text{rad}} = \rho_0 c_0 S \sigma \langle \overline{v^2} \rangle \tag{10.7}$$

where $\langle \overline{v^2} \rangle$ is the spatially averaged mean-square velocity normal to the vibrating surface, ρ_0 is the density of air, c_0 is the speed of sound in air, and σ is a factor called the radiation efficiency. Thus components radiate large amounts of noise if their vibration is large and/or their surface area is large and/or their radiation efficiency is high. The radiation efficiency is usually close to unity at higher frequencies and smaller than unity at low frequencies (where the radiating object is small compared with the wavelength of sound). Predictions of this factor can be obtained using numerical methods such as the boundary element method or, for simple cases, analytical models.

Figure 10.10 shows predictions of the noise from wheels, rails, and sleepers during the passage of a pair of similar bogies. This is shown in the form of the average sound pressure level at a location close to the track (3 m from the nearest rail). The wheel is the most important source of noise at high frequencies, above about 1.6 kHz. From Figure 10.7 it can be seen that this corresponds to the region in which many resonances are excited in the radial direction. Between approximately 400

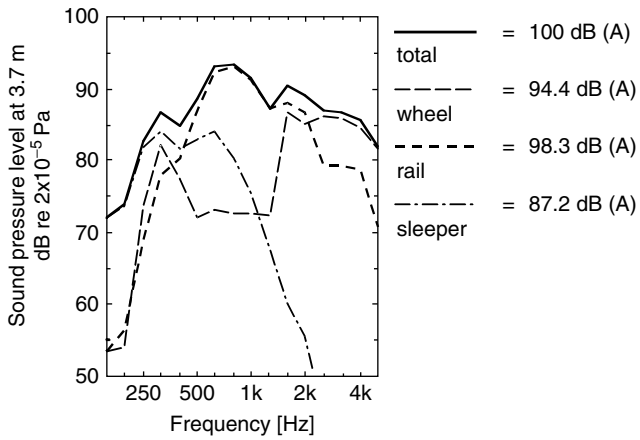

FIGURE 10.10 Predicted noise components from the wheels, rails, and sleepers for 920-mm diameter freight wheels at 100 km/h on a track with moderately soft rail pads.

and 1600 Hz the rail is the dominant source of noise. Here, the rail vibrates at the amplitude of the roughness. The support structure affects the decay with distance and hence the spatially averaged velocity. At low frequencies the sleeper radiates the largest component of noise. Here, the rail and sleeper are well-coupled and have similar vibration amplitudes, but the sleeper has a larger area and a radiation efficiency close to unity, whereas that of the rail reduces below 1 kHz.

Although the details of Figure 10.10 are specific to this combination of wheel and track design, train speed, and roughness spectrum, it is generally the case that the most important source is formed by the sleepers at low frequencies, the rails in the mid frequencies and the wheels at high frequencies. As speed increases the noise spectrum shifts towards higher frequencies, leading to a greater importance of the wheel.

G. Computer Packages

The complete model for rolling noise that has been described in Section II.A to Section II.F has been implemented in a software package, TWINS[12] that is widely used in the industry. This is a frequency-domain model based on the moving irregularity formulation. It produces estimates of sound power and sound pressure spectra in one-third octave bands and allows the user to study the effect of different wheel and track designs on noise.

This model has also been the subject of extensive validation.[13,14] Comparisons between predictions and measurements for three track types, three wheel types, and four speeds gave overall sound levels that agreed within about ± 2 dB.[13] These predictions were updated in Ref. 14, along with new measurements for a range of novel constructions. Revisions to the software have improved agreement slightly. Agreement in one-third octave bands had a larger spread of around ± 4 dB, but this was at least partly due to uncertainties in the measured roughness inputs used in Ref. 13.

III. REDUCING ROLLING NOISE

From the theoretical understanding it is clear that rolling noise can be reduced by:

1. Controlling the surface roughness.
2. Minimising the vibration response of wheels and tracks by adding damping treatments, by shape optimisation of wheels or rails, or by introducing vibration isolation.
3. Preventing sound radiation, for example, by using local shielding measures.

In each case attention must be given to the presence of multiple sources. If more than one source is important, overall reductions will be limited unless all sources are controlled. For example, if there are initially two sources (wheel and track) that contribute equally and one of them is reduced by 10 dB without affecting the other, the overall reduction will be limited to 2.5 dB.

A. Controlling Surface Roughness

From the vehicle designer's point of view, the main feature affecting the wheel roughness is the braking system. Traditional tread brakes, in which cast-iron brake blocks act on the wheel tread, lead to the development of high levels of roughness on the wheel running surfaces due to the formation of local hot spots. This can be seen from Figure 10.3, the greatest differences in roughness being at the peak at approximately 6-cm wavelength. This high roughness in turn leads to higher levels of rolling noise. With the introduction of disc-braked vehicles, for example, the Mk III coach in the U.K. in the mid-1970s, it became apparent that disc braking can lead to quieter rolling stock. The difference in rolling noise between the Mk III and its tread-braked predecessor, the Mk II, was about 10 dB, mainly due to the difference in roughness. Modern passenger rolling stock is mostly disc braked for reasons of braking performance and this brings with it lower noise levels than older stock.

However, environmental noise is usually dominated by freight traffic. Freight vehicles are generally noisier and often run at night when environmental noise limits are tighter. For freight traffic in Europe a number of factors have meant that cast-iron brake blocks have remained the standard. These include cost, the longevity of wagons (typically 50 years), and most importantly, the UIC standards for international operation that have required the use of such brakes. However, since 1999 the UIC has been pursuing an initiative to replace cast-iron blocks with so-called K-blocks.[15] The idea is to introduce blocks made of a composite material that do not produce hot spots and therefore leave the wheel relatively smooth. If possible, these should be available as a "retro-fit" with no further modifications to the vehicles. In practice, the implementation of these blocks has a number of side effects including potentially higher wheel tread temperatures and so the development is ongoing with widespread introduction still a number of years away.

Rail corrugations are also a source of increased noise. A corrugated track can be 10 dB noisier than a smooth one for tread-braked wheels. For disc-braked wheels the difference can be up to 20 dB. Grinding of the rail for acoustic purposes is carried out, for example, in Germany, to maintain special low noise sections of track.

B. Wheel-Based Solutions

1. Wheel Damping

One means of reducing the amount of noise radiated by the wheels is to increase their damping. Impressive reductions in the reverberation of wheels can be achieved by simple damping measures. However, a wheel in rolling contact with the rail is, in effect, already considerably more damped than a free wheel since vibration energy flows from the wheel into the track. To improve the rolling noise performance, the added damping must exceed this effective level of damping, which is one to two orders of magnitude higher than that of the free wheel.

Various devices have been developed to increase the damping of railway wheels by absorbing energy from their vibrations and thereby reducing the noise produced. Examples are shown schematically in Figure 10.11. These include multiresonant absorbers (Figure 10.11a) which have been used in Germany since the early 1980s and are fitted to many trains including the ICE-1. Noise reductions of 5 to 8 dB are claimed for speeds of 200 km/h.[16] Another commercial form of damper involves multiple layers of overlapping plates known as the shark's fin damper (Figure 10.11b). Färm[17] found reductions of 1 to 3 dB(A) overall, associated with wheel noise reductions of 3 to 5 dB(A). Constrained layer damping treatments (Figure 10.11c) consist of a thin layer of

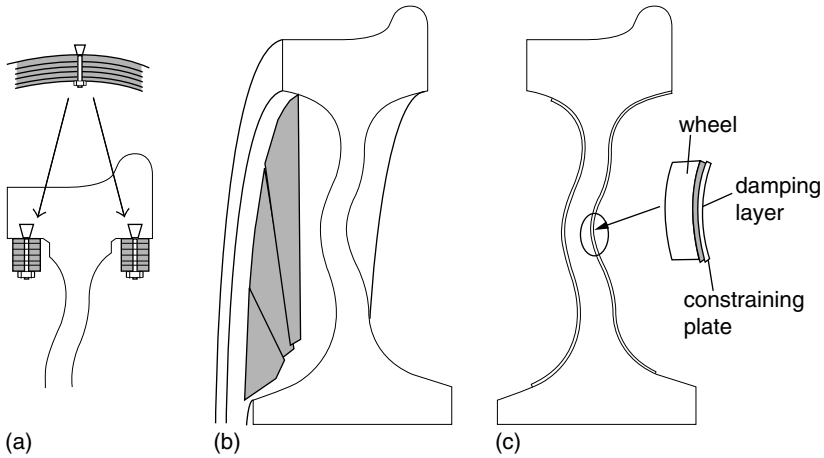

FIGURE 10.11 Various wheel damping devices used on railway wheels: (a) tuned resonance devices, (b) shark's fin dampers, (c) constrained layer damping.

viscoelastic material applied to the wheel and backed by a thin stiff constraining layer (usually metal). Such a treatment was used on the class 150 DMU in the U.K. in the late 1980s and was applied to the whole vehicle fleet to combat a particularly severe curve squeal problem excited by contact between the wheel flange and the check rail. By careful design, sufficient damping can be achieved using constrained layer damping to also make significant reductions in rolling noise.[18,19]

2. Wheel Design

Reductions in the wheel component of radiated noise can also be achieved by careful attention to the wheel cross-sectional shape. In recent years, manufacturers have used theoretical models such as TWINS[12] to assist in designing wheels for low noise.

As an example of the difference that the cross-sectional shape can have, three wheels are shown in Figure 10.12. Wheel (a) is a German Intercity wheel, (b) is a UIC standard freight wheel, and wheel (c) was designed several years ago by the Technical University of Berlin on the basis of scale model testing.[16] Figure 10.12 also shows the predicted noise components from the wheel in each case. The track component of noise (not shown) is not affected by these changes and remains the dominant source up to 1 kHz.

These results show that a straight web (wheel c) is beneficial compared with a curved web (wheel b). This is because the radial and axial motions are decoupled for a straight web. However, it is not always possible to use straight webs if tread brakes are used as the curve is included in the web to allow thermal expansion. Wheel (a) is particularly noisy, the main difference between this and wheel (c) being the transition between the inside of the tyre and the web and the web thickness. Its web is also slightly angled. Increasing the web thickness, and particularly the transition between the tyre and web, are effective means of reducing noise but also lead to increased unsprung mass. It is the case that wheels with profiles similar to (a) have shown appreciable rolling noise reductions by the addition of absorbers, whereas wheels such as (b) have shown much smaller reductions.

Another aspect of wheel design that can be used to reduce noise is the diameter. Smaller wheels have higher resonance frequencies, so it is possible by reducing the diameter to move most of the resonances out of the range of excitation (i.e., above approximately 5 kHz).[20,21] The upper frequency itself is somewhat increased for a smaller wheel due to a shift in the contact patch filter, but this effect is much less significant than the shift in resonance frequencies. The trend in recent years towards smaller wheels for other reasons is therefore advantageous for noise. This also

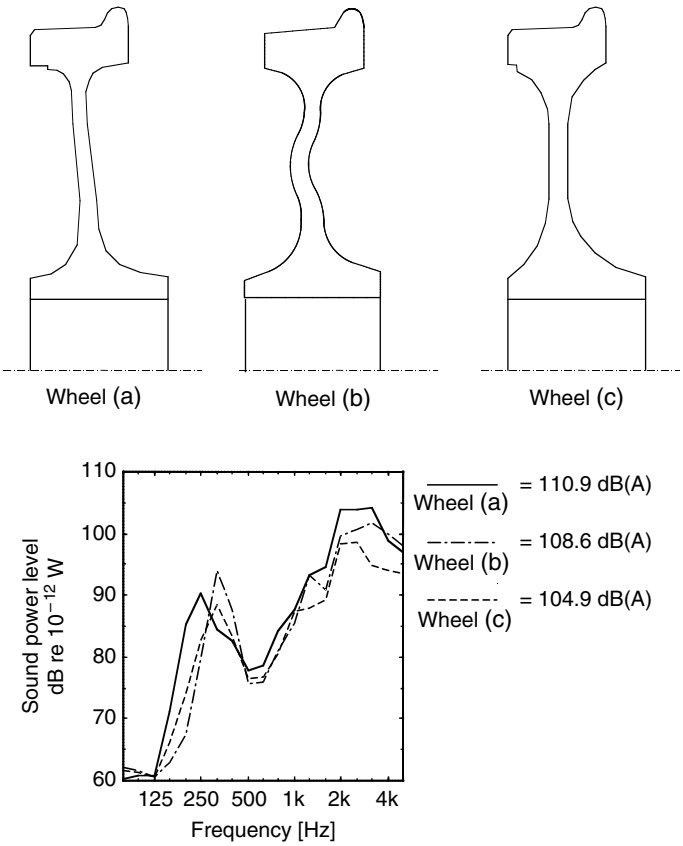

FIGURE 10.12 TWINS predictions of wheel sound power from three types of wheel at a train speed of 160 km/h for the same roughness spectrum in each case, typical of a disc-braked wheel.

negates the increase in unsprung mass caused by increases in thickness. However, if the wheel size is reduced too much, the track noise will increase due to the reduction in contact filter effect.[22]

In the SILENT FREIGHT EU project a shape-optimised wheel was designed that allowed for tread braking.[23] It had a diameter of 860 mm, compared with the reference wheel, which was 920 mm, and it had a somewhat thicker web. The reduction in diameter was limited by the desire to allow retro-fitting to bogies intended for 920 mm wheels. Reductions of 3 dB in wheel component of noise were obtained from these changes.

C. Track-Based Solutions

1. Low Noise Track

To achieve significant reductions in overall noise, it is usually not sufficient to deal only with the wheel noise. There must be a corresponding reduction in noise from the track vibration. Two very important parameters of the track, that affect its noise emission and that are related to one another, are the stiffness of the rail pad and the decay rate of vibrations along the rail. A stiff rail pad causes the rail and sleeper to be coupled together over a wide frequency range. Conversely, a soft pad isolates the sleeper for frequencies above a certain threshold.

The lower the stiffness of the rail pad, the lower this threshold frequency. Soft rail pads therefore effectively isolate the sleepers and the foundation from the vibration of the rail, reducing the component of noise radiated by vibration of the sleepers. Part of the designed role of the rail pad

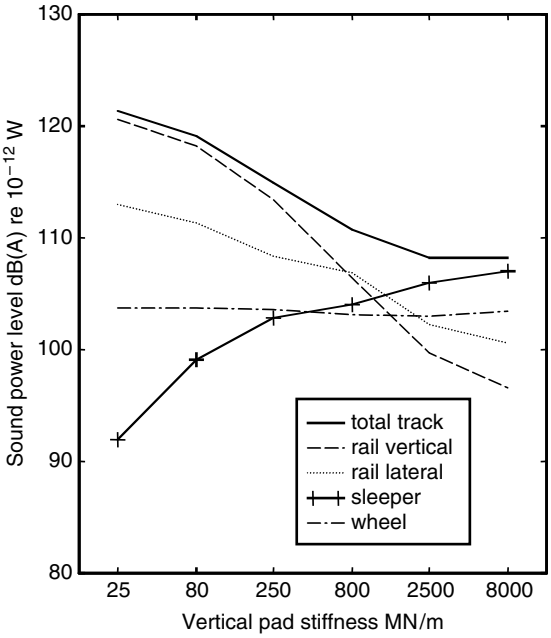

FIGURE 10.13 Effect of rail pad stiffness on predicted components of rolling noise.

is to protect the sleeper and ballast from high impact forces. For this reason softer rail pads have become more commonplace in recent years. Unfortunately, softer rail pads also cause the vibration of the rail to propagate with less attenuation. As a greater length of rail vibrates with each wheel, this means more noise is generated by the rail, as shown in Figure 10.13. There is thus a compromise to be sought between the isolating and attenuating properties of the rail pad.[24]

The recent E.U.-funded research project SILENT TRACK successfully developed and demonstrated low noise technology for the track. The most successful element was a rail damper. Multiple blocks of steel are fixed to the sides of the rail by an elastomer and tuned to give a high damping effect in the region of 1 kHz. This allows a soft rail pad to be used, to give isolation of the sleepers, while minimising the propagation of vibration along the rail.[25]

Figure 10.14 shows the noise reduction achieved in the field tests. In this case, a low noise wheel was used for the comparison to minimise the effect of the wheel on the total noise, but, even so, some wheel noise was present at high frequencies. The overall reduction in *track* noise is approximately 6 dB.

Tests with an optimum pad stiffness have been less successful. Although the effect of pad stiffness has been clearly demonstrated in field tests, the optimum for noise radiation is too stiff to be acceptable for other reasons, particularly track damage protection. Stiff pads are also believed to lead to a higher likelihood of corrugation growth, which in the long term, has a negative effect on the noise. The analysis of the acoustic performance of pads with different stiffnesses is further complicated by their load-dependent characteristics and other factors such as temperature variation.

2. Slab Tracks

Tracks mounted on concrete slabs have become more commonplace in the last few years, notably in Germany on the high speed lines. Such tracks are generally found to be noisier than conventional ballasted track, typically by 3 to 5 dB. This can be attributed to two features of such tracks. First, they tend to be fitted with softer rail fasteners in order to introduce the resilience normally

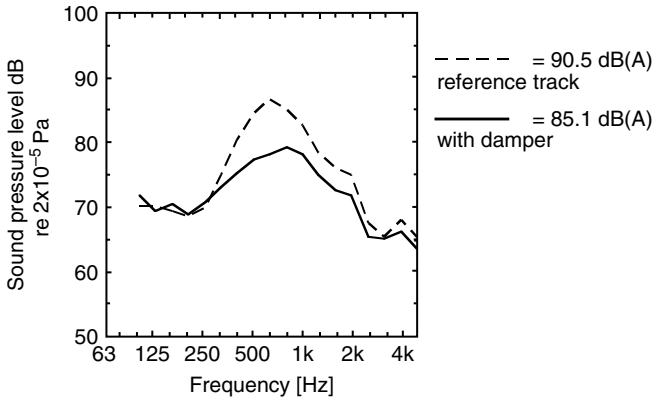

FIGURE 10.14 Measured noise reduction from SILENT TRACK rail damper during the passage of a low noise wheel at 100 km/h.

given by the ballast. Second, they have a hard sound-reflecting surface, whereas ballast has an absorptive effect. The latter affects the overall noise by 1 to 2 dB.

A number of mitigation measures have been studied in Germany, in which absorbent material is added to the upper surface of the slab. This has the effect of reducing the reflections of sound from the slab surface. Where it is also possible to introduce some shielding of the rail noise, for example, by an integrated minibarrier, additional attenuation is possible. Such treatments have been found to reduce noise levels from slab track back to those of ballasted track.

For street-running trams a number of embedded rail systems are used, for example in Manchester, Sheffield, and Birmingham in the U.K. At first sight an embedded rail might be expected to be silent, as the rail is mostly hidden and therefore should not produce sound. In practice, the rail head is visible, and both it and the embedding material around it vibrate and produce sound.

Embedded rail systems offer the possibility of good rail attenuation rates, owing to the damping effect of the embedding material around the rail. They can also be constructed with relatively soft supports and therefore offer the potential to produce good vibration isolation.

D. Local Shielding and Barriers

Another means of reducing the sound radiation is to use a barrier. The efficiency is improved by placing the barrier as close as possible to the source. In the SILENT FREIGHT project, it was demonstrated that, at least for certain types of wheel, a shield mounted on the wheel covering the web can reduce the noise. A more general solution is to place an enclosure around the bogie. If used in combination with low barriers very close to the rail reductions of up to 10 dB can be achieved.[26]

Bogie shrouds and low barriers were also tested in SILENT FREIGHT and SILENT TRACK, but in these cases the objective was to find a combination that satisfied international gauging constraints. Unfortunately, this meant that the overall reduction was limited to less than 3 dB due to the inevitable gap between the top of the barrier and the bottom of the shroud.[27]

There are many other practical difficulties in enclosing the bogies, such as ventilation for the brakes and access for maintenance. Nevertheless, such vehicle-mounted screens are common on trams. Bogie fairings have also been tested on high-speed trains but in this case the objective was to reduce aerodynamic noise.

Conventional noise barriers at the trackside are used widely in some European countries and in Japan. Reductions of 10 to 20 dB are achievable, depending on the height of the barriers, but they

are expensive and visually intrusive especially if taller than about 2 m. Cost-benefit studies have shown that noise reduction at source can be cost-effective compared with barriers or, in combination, can allow the use of lower barriers for the same overall effect.[28]

IV. IMPACT NOISE

A. Introduction

In the previous sections, noise due to random irregularities on the railhead and wheel tread has been considered. As well as this, larger discrete features occur on the running surfaces such as rail joints, gaps at points and crossings, dipped welds, and wheel flats. These cause high interaction forces, and consequently, noise. In some cases loss of contact can occur between the wheel and rail followed by large impact forces. Noise from such discrete features is often referred to as impact noise. Whereas rolling noise can be predicted using a linearised contact spring, in order to predict impact forces and noise the nonlinear contact stiffness must be included, for example, using a Hertzian deflection model (Chapter 4).

Early models for impact noise were essentially empirical.[29] To predict impact forces, time-domain models incorporating the nonlinearities in the contact zone, have been used, for example, by Clark et al.[30] and Nielsen and Igeland.[31] These models contain large numbers of degrees of freedom to represent the track. Nevertheless, they are limited to a maximum frequency of around 1500 Hz. In order to model impact noise up to approximately 5 kHz, simplified models of the wheel and rail have been used in a time-stepping model in order to determine the effects of the nonlinearities.[32] These are then used together with the TWINS model to predict the noise radiation.

B. Wheel Flats

A wheel flat is an area of the wheel tread that has been worn flat, as shown schematically in Figure 10.15a. This usually occurs because the brakes have locked up under poor adhesion conditions at the wheel–rail contact, for example, due to leaves on the railhead during the autumn. Wheels with flats produce high levels of noise and impact loading of the track that can lead to damage of track components. Typically flats can be approximately 50 mm long, in extreme cases up to 100 mm. After their initial formation, flats become worn, i.e., rounded at their ends due to the high load concentration on the corners. A worn flat of a given depth is longer than the corresponding new flat.

Wheel flats introduce a relative displacement input to the wheel–rail system in the same way as roughness. The profile shape can be seen to correspond to a circular arc dip in the railhead.

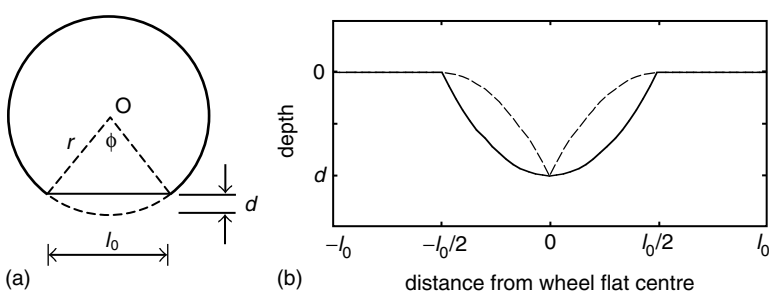

FIGURE 10.15 (a) An idealised flat of length l_0 and depth d; (b) — profile shape, – – – after geometric filtering. *Source*: From Wu, T. X. et al., *J. Sound Vib.*, 251, 115–139, 2002, Elsevier. With permission.

However, owing to the geometry of the wheel and rail surfaces, the actual displacement input is modified by the wheel curvature. For the idealised flat, shown in Figure 10.15a, the wheel first pivots downwards on the front corner of the flat, then pivots upwards again on the rear corner.[32] The resulting relative displacement input experienced by the wheel–rail system is shown in Figure 10.15b. In Ref. 32 it is shown that a worn wheel flat can be represented by a curve of a similar shape to that in Figure 10.15b but elongated.

Figure 10.16 shows examples of the calculated response of the wheel–rail system to a new wheel flat of depth 2 mm (length 86 mm) for a nominal contact force of 100 kN. The model used here represents the wheel as a mass and spring and the track by a simple state-space model fitted to the track mobility.[32]

When the indentation (relative displacement input due to the wheel flat) appears between the wheel and rail, the wheel falls and the rail rises. Since the wheel and rail cannot immediately follow the indentation owing to their inertia, the contact force is partly unloaded. At a train speed of 30 km/h (Figure 10.16a), full unloading first occurs.

After the relative displacement input reaches its maximum, the contact force increases rapidly until it reaches its peak (the wheel is now pivoting about the trailing edge of the flat). The peak force is here about four times as large as the static load. As the speed increases, contact is lost for longer periods during the unloading phase. At 80 km/h (Figure 10.16b), a second loss of contact can be seen to occur. However, the second impact is much smaller than the first one.

Comparisons with measured impact forces[33] suggest that the simplified geometry indicated in Figure 10.15 leads to overestimates of the contact force. Measured wheel flat profiles are required to give more accurate predictions.

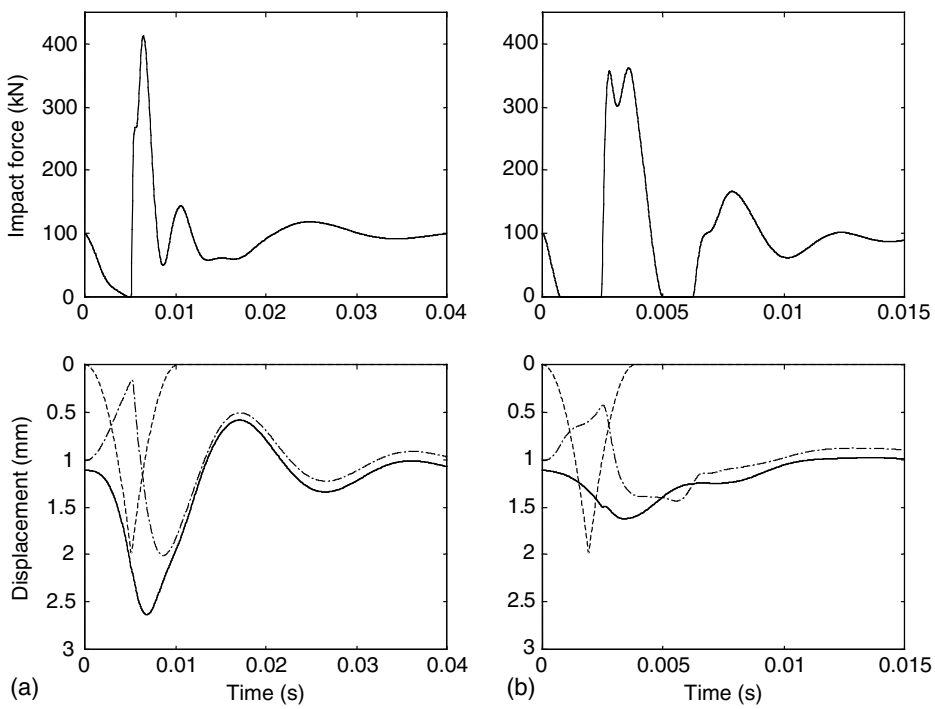

FIGURE 10.16 Predicted wheel–rail interaction and displacements of wheel and rail due to 2 mm newly formed wheel flat. (a) At train speed 30 km/h; (b) at 80 km/h: — wheel displacement, – – – rail displacement, … relative displacement excitation. *Source*: From Wu, T. X. et al., *J. Sound Vib.*, 251, 115–139, 2002, Elsevier. With permission.

C. Predicting Impact Noise from Wheel Flats

It is not possible to use the contact force obtained from the impact model and apply it directly within the TWINS model, because the predicted interaction force is very sensitive to details of the wheel and track dynamics used in its prediction. With a modal wheel model, the force will have strong dips at the wheel resonance frequencies. The wheel response has only shallow peaks, just above the resonance frequencies. The interaction with the track thereby introduces apparent damping to the wheel.

A hybrid approach has therefore been developed,[32] whereby an equivalent roughness spectrum is derived. This is defined such that the contact force spectrum obtained using the above *nonlinear* model is identical to that obtained using a *linear* model excited by the equivalent roughness spectrum. At this stage the wheel and track are represented by the same simple elements as above in both cases. The equivalent roughness spectrum can then be used as the input to a more detailed linear frequency-domain model, such as the TWINS model, to predict the noise due to the impact.

Example results are given in Figure 10.17a. This shows the sound power due to one wheel and the associated track vibration for a 2-mm deep new wheel flat at different speeds for 100 kN wheel load. Results correspond to the average over a whole wheel revolution. Figure 10.17b shows, for comparison, corresponding results for roughness excitation due to a moderate roughness (tread-braked wheel roughness). As the speed increases, the noise at frequencies above approximately 200 to 400 Hz increases in both cases. The increase in rolling noise with increasing speed is greater than that due to the flat. For the wheel flats considered here, the noise generated exceeds that due to the tread-braked wheel roughness at all speeds and in all frequency bands, although the noise due to roughness increases more rapidly with speed so that at sufficiently higher speeds it can be expected to dominate. For corrugated track, the noise due to roughness exceeds that due to wheel flats at 120 km/h.

Figure 10.18 provides a summary of the variation of the overall A-weighted sound power level with train speed. The predicted noise level due to conventional roughness excitation increases at a rate of approximately 30 $\log_{10}V$, where V is the train speed, whereas the noise due to flats increases at an average of around 20 $\log_{10}V$ once loss of contact occurs. For example, loss of contact was found to occur for the newly formed 2-mm deep flat at speeds above 30 km/h and for a rounded 2-mm flat above 50 km/h. This variation with speed indicates that the radiated sound due to wheel flats continues to increase with increasing speed, even though loss of contact is occurring.

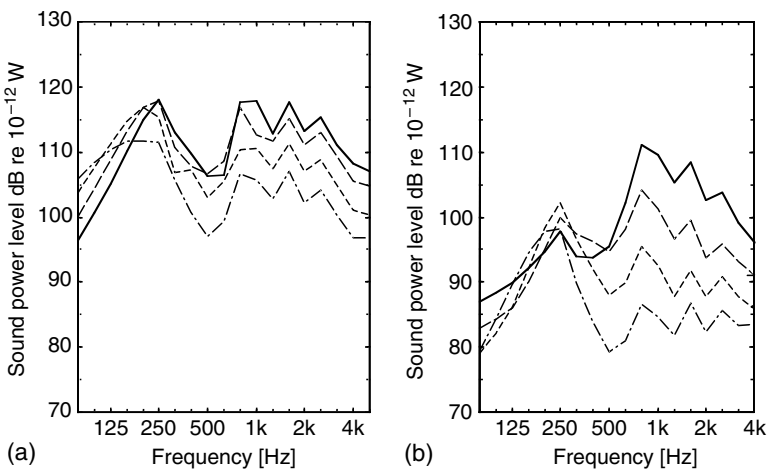

FIGURE 10.17 Sound power level due to wheel and track: (a) 2 mm new wheel flat; (b) rolling noise from moderate roughness. –. –. – 30 km/h, … 50 km/h, – – – 80 km/h, — 120 km/h. *Source*: From Wu, T. X. et al., *J. Sound Vib.*, 251, 115–139, 2002, Elsevier. With permission.

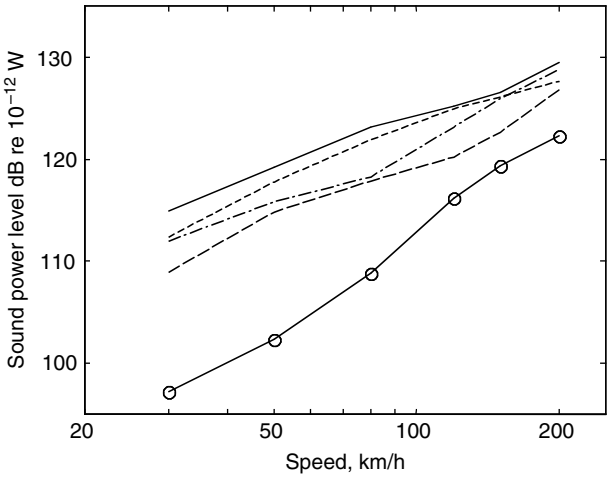

FIGURE 10.18 Sound power radiated by one wheel and the associated track vibration: – – – 1 mm rounded flat, … 2 mm rounded flat, –. –. – 1 mm new flat, — 2 mm new flat, o—o rolling noise due to tread-braked wheel roughness. *Source*: From Wu, T. X. et al., *J. Sound Vib*., 251, 115–139, 2002, Elsevier. With permission.

Impact noise from wheel flats is found to depend on the wheel load. The increase in noise between a load of 50 and 100 kN is about 3 dB. In contrast, the rolling noise due to roughness is relatively insensitive to wheel load.

D. Rail Joints

In a similar way to wheel flats, rail joints provide discrete inputs to the wheel–rail system that induce quite large contact force variations. Rail joints can be characterised by a gap width and a step height (either up or down) (see Figure 10.19a). Moreover, the rail often dips down to a joint on both sides (Figure 10.19b). Such dips are also present at welds, and are usually characterised in terms of the angle at the joint.

A similar approach has been used as that above to study the effects of rail joints.[34,35] The sound radiation was calculated using the same hybrid method as for the wheel flats. It was found, for realistic parameter values, that the gap width is insignificant compared with the step height and dip angle.

Results are shown in Figure 10.20a for undipped rail joints in the form of the total A-weighted sound power emitted by the wheel and rail during 1/8 sec. The results for a step-down joint are found to be virtually independent of the step height (only results for one value are shown) and also change very little with train speed. However, for step-up joints both the peak contact force and the sound power level increase with step height and with train speed. The sound power level from a single joint has a speed dependence of around 20 $\log_{10}V$.

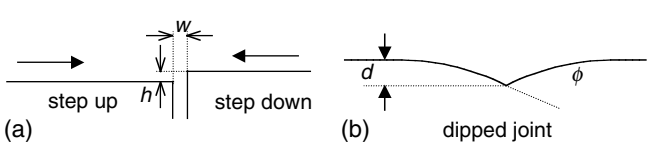

FIGURE 10.19 Idealised rail joints showing (a) step height h and gap width w, (b) dip height d and angle ϕ.

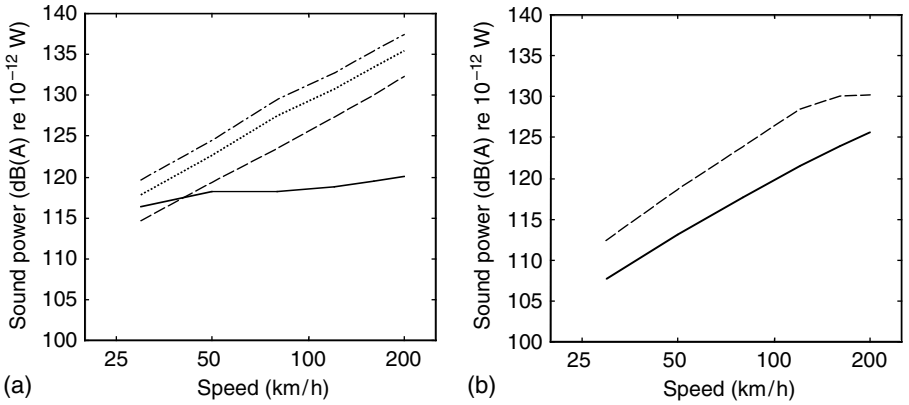

FIGURE 10.20 A-weighted sound radiated by one wheel and the associated track vibration during 0.125 sec due to a wheel passing over: (a) flat rail joints, – – – 1 mm step-up, … 2 mm step-up, –. –. – 3 mm step-up, — 2 mm step-down; (b) dipped rail joints with no height difference, — 5 mm dip, –. –. – 10 mm dip (all with 7 mm gap).

In Figure 10.20b, results are given for dipped joints with no height difference. Here a dip of 5 or 10 mm is considered as a quadratic function over a length of 0.5 m either side of the joint. A dip of 5 mm corresponds to a joint angle of 0.04 rad which is large although within a typical range, a dip of 10 mm corresponds to 0.08 rad which is severe. The 10-mm dip produces a similar noise level to a 1-mm step-up undipped joint, although for speeds above 120 km/h the noise level from the dip joint becomes independent of train speed.

Figure 10.21 shows the predicted noise for joints with both dipped rails and steps. The noise radiation generally increases with speed, regardless of whether loss of contact occurs. For the 5-mm dip, the noise level increases by 8 dB when the step height increases from 0 to 2 mm. For the step-down joints, the noise level is higher than without a step, although at higher speeds the dip has more effect than the step. The results for the 10-mm dip are similar for both step-up and step-down joints, indicating the dominance of the dip in this case.

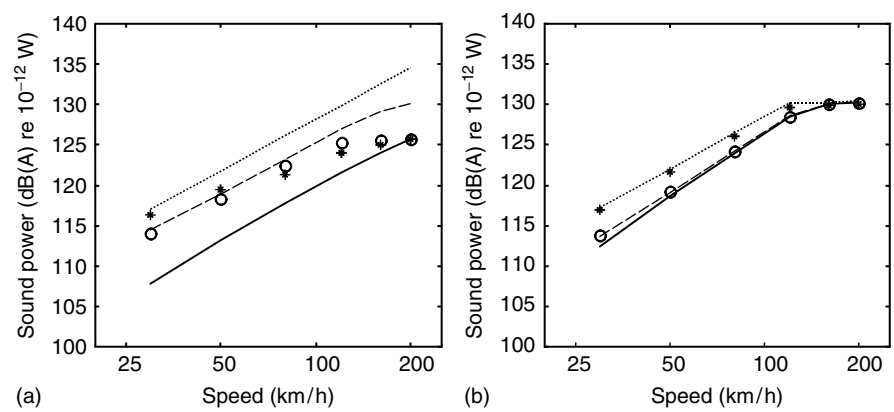

FIGURE 10.21 A-weighted sound power radiated by one wheel and the associated track vibration during 0.125 sec due to a wheel passing over different rail joints with 7 mm gap and 5 or 10 mm dip: (a) for 5 mm dip; (b) for 10 mm dip. … 2 mm step-up, – – – 1 mm step-up, — no height difference, * 2 mm step-down, o 1 mm step-down.

To compare these results with typical rolling noise results, the time base of the joint noise should be adjusted to the average time between joints. This shows[34] that rolling noise due to the tread-braked roughness considered above is similar to the average noise due to 5-mm dipped joints with no height difference (Figure 10.20b). With a height difference of 2 mm the average noise predicted from the joints increases to almost 10 dB greater than the rolling noise. Moreover, since the time between rail joints decreases as train speed increases, it is also found that the average noise level from joints increases at about 30 $\log_{10}V$, similar to rolling noise.

E. Reducing Impact Noise

In order to reduce impact noise it is clearly desirable to remove the cause, if this is possible. Wheel flats can be largely prevented by installation of wheel-slide protection equipment. Monitoring equipment is now widely used to identify wheels with flats, to allow them to be removed from service as quickly as possible for reprofiling. On main lines, jointed track has been mostly replaced by continuously welded rail in the last 30 years, although inevitably, joints such as expansion joints, track-circuit insulating joints, and points and crossings remain. Even so, measures such as swing-nose crossings allow the impact forces, and thus noise, to be minimised. Attention should also be given to ensuring that welded rail joints are as level as possible by using rail straightening equipment.

As the mechanism of impact noise is a vertical relative displacement excitation, countermeasures that are effective for rolling noise, such as are discussed in Section III, can be expected to work equally well for impact noise. This includes, for example, wheel damping, wheel shape optimisation, rail damping, and local shielding.

V. CURVE SQUEAL

A. Mechanism of Squeal Noise Generation

Railway vehicles travelling around tight curves can produce an intense squealing noise. This is a particular problem where curved track exists in urban areas and it has been found to be annoying to both residents and railway passengers.

When a railway wheelset in a bogie traverses a curve it is unable to align its rolling direction tangentially to the rail (Figure 10.22). In sharp curves, this misalignment leads to large creep forces at the wheel–rail interface. The leading inner wheel of a bogie has its contact point with the rail towards the field side of the tread and experiences high lateral creepage. The leading outer wheel tends to be in flange contact, with the resultant lateral force acting inwards to ensure that the wheelset remains on the track. Longitudinal and spin creep forces also act as shown in Figure 10.22.

Figure 10.23a shows a typical "creep curve" relating creep force to creepage. At low values of creepage the magnitude of the creep force increases linearly. At high values of creepage the force becomes saturated, with a maximum value of $\mu_0 N$, where μ_0 is the friction coefficient and N is the normal load. In practice, however, the friction coefficient μ is not a constant. It is usually recognised that dynamic or sliding friction coefficients are smaller than static ones. In fact, the friction coefficient depends on the sliding velocity, decreasing as the velocity increases. Thus, as creepage increases beyond the saturation point, the creep force once more reduces in amplitude (see Figure 10.23b). It is this falling amplitude at high creepage that is believed to be the main reason for the unstable dynamic behaviour leading to squeal noise.

By analogy with a damper, which gives a reaction force that is proportional to the relative velocity, the falling creep curve can be considered as a negative damping. Thus, the reaction force decreases as the relative velocity increases. Since wheel modes have very low levels of damping (see Section II), if this negative damping exceeds a certain level, it causes instability of the wheel modes making them prone to squeal.

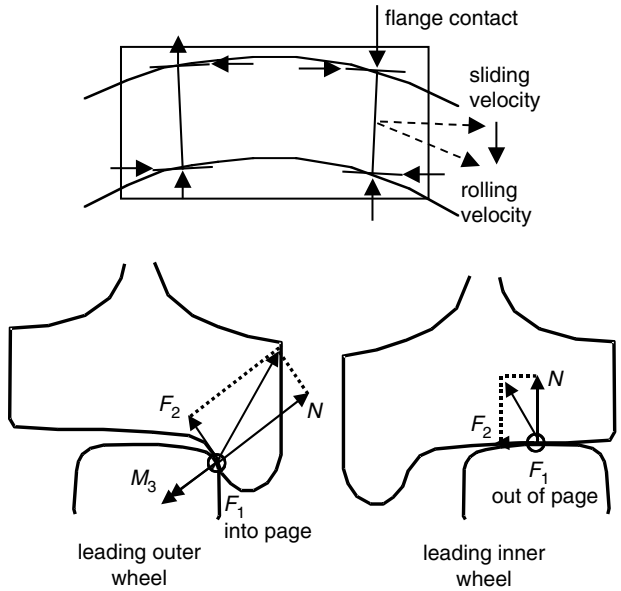

FIGURE 10.22 Schematic view of forces acting on wheels of a bogie in a curve. N is normal load, F_2 is lateral creep force, F_1 longitudinal creep force, and M_3 is spin moment.

There are two main types of curve squeal, characterised by the mechanisms of excitation:

1. Stick–slip excitation owing to lateral slip of the wheel due to its alignment.
2. Squeal due to wheel flange contact with the rail.

Observations indicate that the highest squeal noise amplitude is usually generated by the *leading inner* wheel of a four-wheeled bogie or two-axle vehicle. This noise is associated with stick–slip lateral motion at the contact between the wheel and the rail. The fundamental frequency of such squeal noise corresponds to a natural frequency of the wheel and is often in the range 200 to 2000 Hz. The wheel modes excited in this case are axial modes with no nodal circle and their maximum amplitude at the wheel tread (see first row of Figure 10.6).

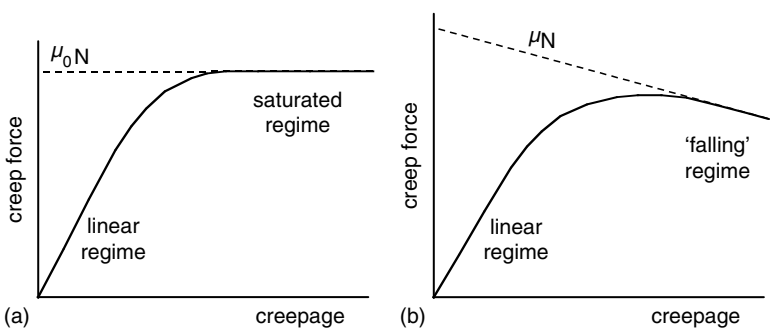

FIGURE 10.23 A typical creep force-creepage relationship: (a) for constant friction coefficient; (b) for velocity-dependent friction coefficient.

Contact between the wheel flange and the rail, which occurs at the *leading outer* wheel (and possibly the *trailing inner* wheel) in sharp curves, has generally been found to reduce the likelihood of stick–slip squeal due to lateral slip at this wheel. For example, Remington[36] concluded from laboratory experiments that flange contact reduces the level of squeal noise. However, it is thought that flange contact may generate a different form of squeal noise. Compared with squeal due to lateral slip, this generally has a considerably higher fundamental frequency, may have a lower level, and is often more intermittent in nature. Nevertheless, it can be a source of considerable annoyance. It is usually associated with flange contact; either with the outer running rail, with check rails in sharp curves, or wing rails in points and crossings. Compared with squeal due to lateral slip, flange noise has received much less attention.

Theoretical models for curve squeal have been developed by various authors. Rudd[37] (see also Remington[36]) indicated that instability of the lateral friction force was the most likely cause of squeal and gave a simple model. Fingberg[38] and Périard[39] have extended this basic model by including better models of the wheel dynamics, the friction characteristic, and the sound radiation from the wheel. Time-domain calculations allowed the squeal magnitude to be predicted as well as the likelihood of squeal to be determined. Heckl[40] also studied squeal using a simplified model and provided experimental validation using a small-scale model wheel.

De Beer et al.[41] extended these models, based on excitation by unstable lateral creepage, to include feedback through the vertical force as well as through the lateral velocity. Their model consists of two parts: a first part, in the frequency domain, can be used to determine instability and to predict which mode is most likely to be excited, and a second part, in the time domain, calculates the amplitude of the squeal noise.

This model has been extended further to allow for an arbitrary contact angle and to include lateral, longitudinal, and spin creepage.[42] This allows it to be applied to flange squeal as well as squeal due to lateral creepage.

B. Reducing Squeal Noise

In discussing solutions for curve squeal it is of little value to quote decibel reductions. The nature of the instability is such that effective measures usually eliminate the squeal rather than reduce it. Curve squeal tests are also extremely unreproducible due to a high sensitivity to parameters such as temperature, humidity, train speed, track geometry, and wheel and rail wear.

Known solutions for curve squeal include lubrication using either grease or water or the application of friction modifiers that reduce the difference between static and sliding friction coefficients. If lubricants are used, it must be ensured that they do not lead to loss of adhesion as this could compromise safety. Grease is therefore only applied to the rail gauge corner or wheel flange. Although this may not be the primary cause of squeal noise, by modifying the curving behaviour this can nevertheless reduce the occurrence of squeal. Water sprays have also been used effectively in a number of locations.

Friction modifiers act by reducing or eliminating the falling friction characteristic without reducing the level of friction. These can be applied either to the track at the entrance to a curve, or on the vehicle. They have been shown to be very effective in eliminating squeal and can be applied to the top of the railhead without compromising traction or braking.[43]

Wheel damping treatments are also known to reduce the occurrence of squeal. In this case a small increase in the level of damping can be effective in eliminating squeal. In addition to the forms of damping discussed in Section III.B, ring dampers have been used as a simple means of increasing the damping of a wheel.[44,45]

Effective solutions can also be sought in the design of vehicles for curving in order to reduce the creepages. Unfortunately, this is often in conflict with the design of bogies for stability at high speed.

VI. OTHER SOURCES OF NOISE

A. Aerodynamic Noise

Aerodynamic sound sources increase in sound power more rapidly with speed than mechanical sources. For an aeroacoustic monopole source, such as the pulsating flow from an exhaust pipe, the sound power increases with flow speed according to the fourth power of the speed. This means that the sound power level increases at a rate of 40 $\log_{10}V$. For a dipole-type source, such as the tones generated by vortex shedding from a cylinder or turbulence acting on a rigid surface, the rate is 60 $\log_{10}V$, whereas for a quadrupole source such as free turbulent flow the rate is 80 $\log_{10}V$.

Aerodynamic sources become dominant for exterior noise of trains above a speed of approximately 300 km/h. Below this speed noise levels increase at about 30 $\log_{10}V$ (typical of rolling noise) whereas above this speed they increase at a rate of 60 $\log_{10}V$ or more.[46]

Where noise barriers are placed alongside the track, the wheel–rail noise may be attenuated by 10 to 15 dB, while leaving the aerodynamic sources from the upper part of the train and pantograph exposed. This causes aerodynamic noise to become important at lower speeds. Aerodynamic sources are also important for interior noise in high-speed trains, particularly the upper deck of double-deck trains where rolling noise is less noticeable.

Turbulent airflow, which can be caused by many different parts of a rail vehicle, is an important source of aerodynamic noise.[47] The locations of a number of sources have been identified and their strengths quantified in studies using specialised microphone arrays.[48] Important sources are found to fall into two main categories.[49] The first category, which is dipole in nature, is generated by airflow over structural elements: the bogies, the recess at the intercoach connections, the pantograph and electrical isolators on the roof, and the recess in the roof in which the pantograph is mounted. In addition, the flow over the succession of cavities presented by louvred openings in the side of locomotives is a source of aerodynamic noise, the form of which depends on the length and depth of the cavity. In the second category, which may have a dipole or quadrupole nature, noise is created due to the turbulent boundary layer.

Empirically based models for each source of aerodynamic noise from trains can be derived if the locations and source strengths are experimentally determined. Measurements may be complemented by the use of computational fluid dynamics (CFD) models. While a working theoretical model for the aerodynamic sources from trains is not yet available, it is the objective of current research.[49]

B. Power Unit Noise

Power units on trains are generally either electric or diesel. Noise from diesel locomotives is mostly dominated by the engine and its intake and exhaust. Space restrictions often limit the ability to silence the exhaust adequately, although in modern locomotives this has been given serious attention. On electrically powered stock, and on diesels with electric transmission, the electric traction motors and their associated cooling fans are a major source of noise. Most sources of noise from the power unit are largely independent of vehicle speed, depending rather on the tractive effort required. The whine due to traction motors is an exception to this.

VII. VEHICLE INTERIOR NOISE

A. Vehicle Interior Noise Levels

All the noise sources discussed above are also of relevance to interior noise in trains.[50] Noise is transmitted from each of these sources to the interior by both airborne and structure-borne paths, with structure-borne transmission often dominant at low frequencies and airborne transmission at high frequencies. The noise from the wheel–rail region is often the major source. Additionally, on

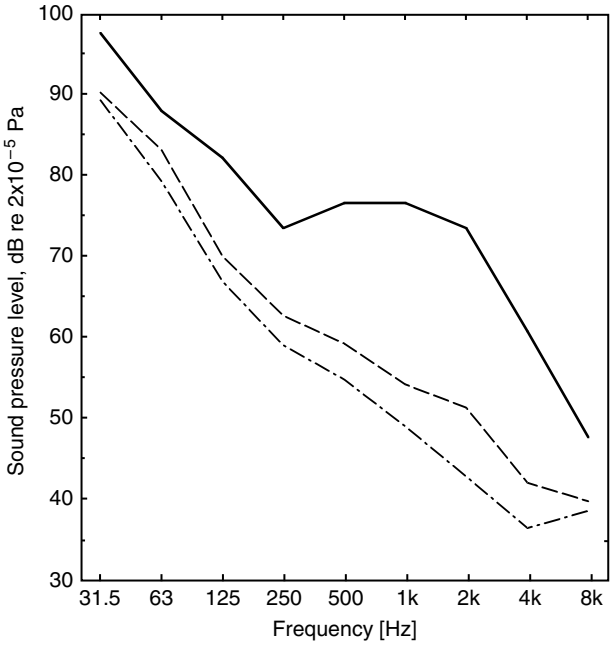

FIGURE 10.24 Octave band spectra measured inside British rolling stock at 145 km/h (from Ref. 51). — Mk 1 vehicle (81 dB(A)), – – – Mk 2d vehicle (63 dB(A)), –. –. – Mk 3 vehicle (59 dB(A)).

vehicles with underfloor diesel engines, noise from the engine can be significant. Noise from the air-conditioning system, where this is present, can also require consideration in rolling stock. There is often very limited space in which to package the air-conditioning unit and ducts.

Examples of noise spectra inside British vehicles are shown in Figure 10.24 (taken from Eade and Hardy[51]). The Mk 1 vehicle was constructed in 1960 and had opening windows; the Mk 2d coach was introduced in 1970 and had sealed windows and air-conditioning; the Mk 3 coach was introduced in 1975 and has a similar interior to the Mk 2d but has disc brakes. The more modern stock can be seen to produce a considerable improvement at higher frequencies, but the differences at low frequencies are much more modest so that the low frequency noise now accounts for a much higher proportion of the total.

Other results are given in Figure 10.25 and Figure 10.26. The results in Figure 10.25 show that modern high-speed trains are quieter at 300 km/h than a conventional "rail car" at a lower speed.[52] Figure 10.26 shows measured spectra in an open saloon coach both in the open and in a tunnel.[53] The noise levels can be seen to increase considerably in the mid-frequency range in a tunnel owing to a greater contribution from the walls, windows, and roof.

B. Measurement Quantities for Interior Noise

Conventionally, the A-weighted sound pressure level has been used to specify acceptable levels inside vehicles. Internationally agreed limits are 68 dB(A) in second class and 65 dB(A) in first class.[53] However, as seen above, the spectrum of noise inside trains contains considerable energy at low frequency. This low frequency sound energy can be a source of human fatigue, but is not effective in masking speech, for which noise in the range 200 to 6000 Hz is most effective.

Passenger requirements for noise inside a train vary from one person to another.[54] Clearly, it is desirable that the noise should not interfere with conversation held between neighbours. However, particularly for a modern open saloon-type vehicle, silence would also not be the ideal.

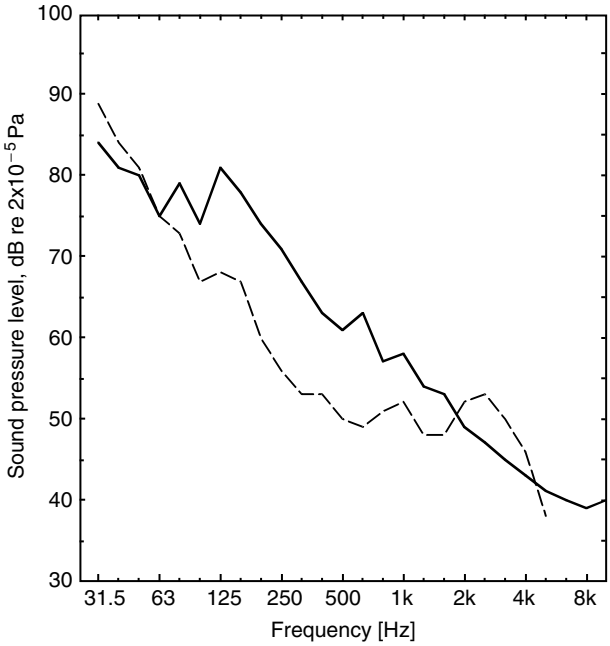

FIGURE 10.25 One-third octave band spectra measured inside French rolling stock (from Ref. 52). — railcar at 160 km/h (72 dB(A)), – – – TGV at 300 km/h (64 dB(A)).

There should be sufficient background noise so that passengers talking do not disturb other passengers further along the vehicle (people talking loudly into mobile phones are a particular source of annoyance). According to Ref. 55, for example, the interior noise level should be at least 60 dB(A) to avoid disturbance by other passengers.

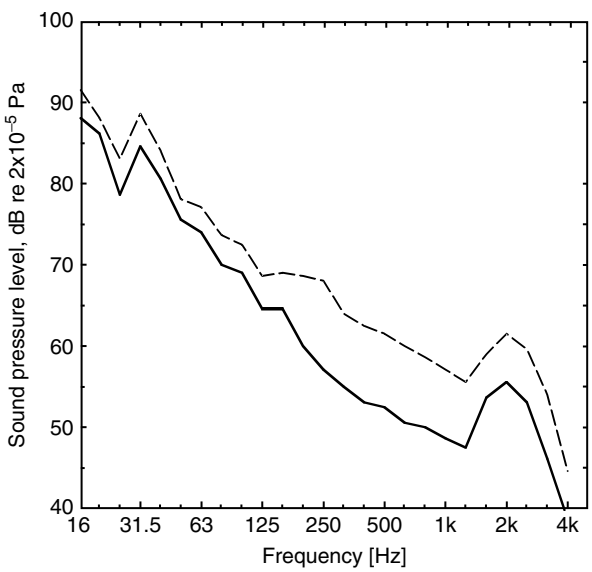

FIGURE 10.26 One-third octave band spectra measured inside German rolling stock at 200 km/h on ballasted track (from Ref. 53). — in the open (64 dB(A)), – – – in tunnel (71 dB(A)).

Various alternative quantities exist that can be used to define acceptable environments. These include the B-weighted level, preferred speech interference level (PSIL), loudness level, alternative noise criteria (NCA), noise ratings (NR), and room criteria (RC).[51,56]

The interior sound level varies considerably within a vehicle. Figure 10.27 shows some examples of measured results where a loudspeaker has been placed at one end of an open saloon vehicle. This was a Mk 2 coach dating from the 1960s, although the interior dated from the 1990s. The solid line shows the relative sound pressure along a line down the central gangway at the height of the headrests. Results are shown in three example one-third octave bands. At low frequencies, strong modal patterns are observed due to the long acoustic wavelength. At higher frequencies considerable decay in the sound level is observed along the coach due to the absorptive properties of the seats, carpets, etc. Additional attenuation is seen at the middle of the coach where two glass partial screens were present either side of the door.

Also shown are measured results at positions in front of each seat headrest. The seats were arranged in groups of four with tables in between them. At low frequencies these measurements follow the same pattern as the gangway measurements, but at higher frequencies considerable differences can be seen between adjacent seated positions. These spatial variations may be experienced by passengers in the vehicles — the 500 Hz frequency band, for example, is quite important for speech interference. It can also be expected that differences will occur between left and right ear positions at an individual seat, leading to binaural effects. Clearly, in a running vehicle other source positions will apply, but these results serve to illustrate the general trends that can be expected.

C. Airborne Transmission

Airborne sound transmission into the vehicle occurs due to acoustic excitation of the vehicle floor, walls, windows, doors, and roof. The acoustic performance of a panel can be measured by placing it between two reverberant rooms and measuring the difference in sound pressure level between the two rooms.[3] The sound reduction index (or transmission loss) is the difference between the incident intensity level and the transmitted intensity level that can be derived from such a measurement after allowing for the size of the panel and the absorption in the receiver room.

A typical sound reduction index of a homogeneous panel is shown in Figure 10.28. Generally, the sound reduction index of panels is dominated by the "mass law" behaviour in a wide frequency range. At high frequencies, the coincidence region occurs where the wavelengths in the structure and in air are similar. Here, a dip in the sound reduction index occurs, the extent of which depends on the damping. The mass law behaviour extends from the first resonance of the panel up to just below the critical (or coincidence) frequency. In this region the bending stiffness of the panel and its damping have no effect on the sound transmission (see Ref. 3 for more details).

The use of light-weight constructions such as extruded aluminum or corrugated steel leads to a low sound reduction index. This follows from the mass law, which states that the sound reduction index reduces by 6 dB for a halving of panel mass. However, such structures tend to have a performance that is even worse than the mass law would suggest due to the presence of an extended frequency region over which coincidence effects occur. For example, Figure 10.29 shows measurements of the sound reduction index from a 60-mm thick extruded aluminum floor of a railway vehicle with a 3-mm wall thickness taken from Ref. 57 (similar results are also found in Ref. 58). Also shown is the "field incidence" mass law estimated for a homogeneous panel of similar mass.[3] Clearly, the extruded panel exhibits a much lower sound reduction index than this. It can be brought closer to the mass law behaviour by the use of a suspended inner floor and by adding a damping treatment to the extruded section.

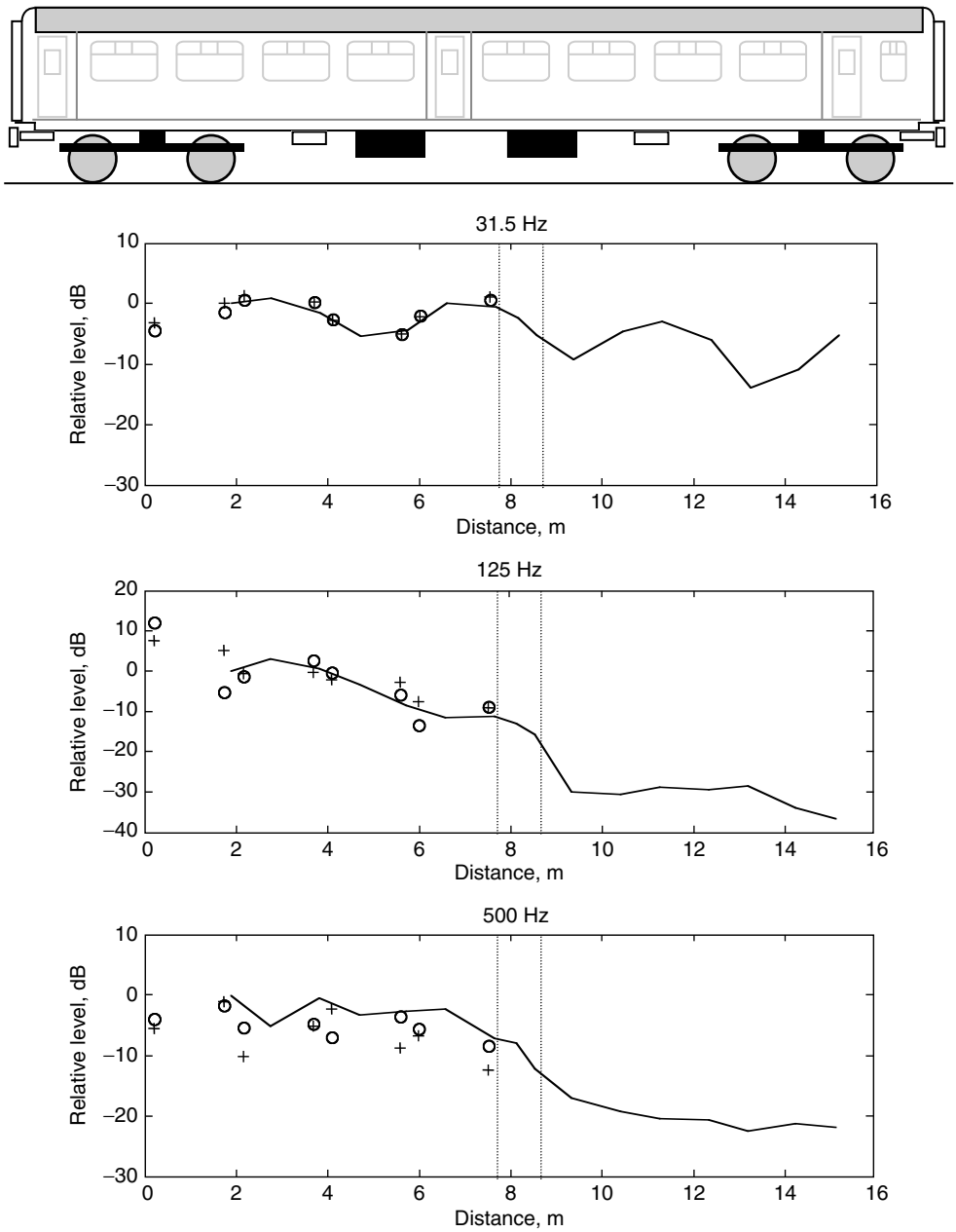

FIGURE 10.27 Relative internal sound levels in selected one-third octave bands in an ex-BR Mk 2 coach due to a sound source located at the left-hand end, 1.05 m above the floor. — measured at 1.05 m from floor along central gangway, o measured 0.05 m from head-rests of aisle seats (height 1.05 m from floor), + measured 0.05 m from headrests of window seats (height 1.05 m from floor). Positions of partial screens indicated by dotted lines.

D. Structure-Borne Transmission

As well as the airborne path, considerable sound power is transmitted to the vehicle interior through structural paths. This originates from the wheel–rail region as well as from underfloor diesel

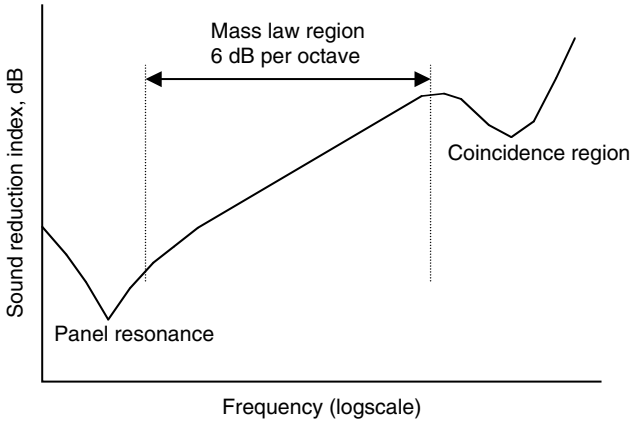

FIGURE 10.28 Typical sound reduction index of a homogeneous panel due to a diffuse incident field.

engines where these are present. Structure-borne engine noise could be reduced significantly in many cases by applying good mounting practice.[50] The mount stiffness must be chosen taking into account the frequency characteristics of the engine. An incorrect choice of stiffness can lead to amplification rather than attenuation of transmitted vibration. Flanking paths via pipes and hoses should also be avoided.

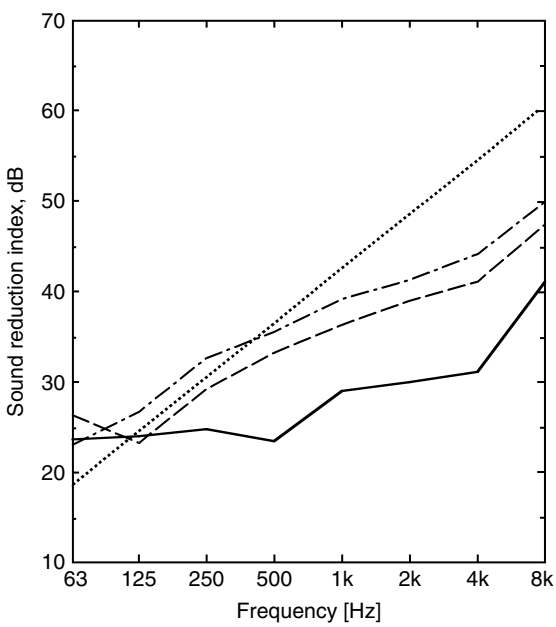

FIGURE 10.29 Octave band sound reduction index of extruded aluminum floor. — measured on bare floor panel, … field incidence mass law for 30 kg/m^2,– – – measured for bare floor panel plus 12 mm suspended wooden deck, –. –. – measured for damped floor panel plus 12 mm suspended wooden deck (data taken from Ref. 57).

E. Prediction of Interior Noise

Deterministic methods, such as finite elements (FEM), may be applied at low frequencies to predict the vehicle interior noise.[59] Owing to the regular geometry an analytical model of the interior may also be used to construct the interior acoustic field on the basis of simple room modes.[60]

However, at high frequencies the number of modes becomes prohibitive for such approaches. The preferred analysis method for frequencies above approximately 250 Hz is therefore statistical energy analysis (SEA). This can be used in both predictive[57,61] and experimental modes.[62] However, in predictive mode it is not straightforward to define the coupling loss factors between the various subsystems, especially where use is made of aluminum extrusions[58,63,64] or other inhomogeneous constructions.[65] This is an area of continuing research. Moreover, as SEA is a statistical method, it provides an average result and cannot account easily for the spatial variations in sound field such as seen in Figure 10.27.

VIII. GROUND-BORNE VIBRATION AND NOISE

A. Overview of Vibration Phenomena

Just as environmental noise is receiving increased attention, so is the related environmental issue of ground vibration from rail traffic. Three distinct effects of ground vibration may be identified that arise predominantly from different types of railway.

Heavy axle-load freight traffic, travelling at relatively low speeds, causes vibration at the track of high amplitude that excites surface-propagating waves in the ground. This type of vibration often has significant components at very low frequency (below 10 Hz) and may interact with the frequencies of buildings rocking or bouncing on the stiffness of their foundations in the soil. This phenomenon is especially associated with soft soil conditions where it is found that significant levels of vibration may be propagated up to distances of the order of 100 m from the track. At these frequencies the vibration is perceived in the building as "whole body" vibration, which can be felt. This is usually assessed under the principles of ISO 2631.[66] High levels of vibration cause annoyance and, possibly, sleep disturbance. Complaints are often expressed in terms of concern over possible damage to property, although, for the levels of vibration normally encountered from trains, such concern is unlikely to be borne out when assessed against the criteria for building damage, e.g., BS 7385[67] or DIN 4150.[68]

Passenger trains also may cause significant levels of vibration, particularly electric multiple units with high unsprung masses. However, at sites of mixed traffic it is usually the case that a few freight trains, perhaps running at night, are identified as the worst cases and it is these which dominate the assessment of potential annoyance.

High-speed passenger trains sometimes travel at speeds in excess of the speed of propagation of vibration in the ground and embankments. This has been the concern of track engineers for some years because of the large displacements that can be caused in the track support structure and in electrification masts, etc. For its effect in causing ground vibration that propagates away from the track, this phenomenon may be compared with the bow wave from a ship or, more sensationally, the "boom" from a supersonic aircraft. Although the occurrences of this are comparatively rare, the topic has attracted considerable attention among researchers recently because of the expansion of the network of high-speed railways.[69–71] Hence, high-speed railways may also cause significant levels of surface vibration propagating to comparatively large distances from the track.

The third effect arises where trains run in tunnels and vibration is transmitted to buildings above. This has higher frequency content than vibration from surface tracks/trains. Although no direct airborne noise can be heard, vibration at the low end of the audible frequency range, from approximately 30 to 200 Hz, may excite bending in the floors and walls of a building which then radiate noise directly into the rooms. This rumbling noise may be found to be all the more annoying

because the source cannot be seen and no screening remedy is possible. This ground-borne noise is dealt with using soft baseplates, floating slab track, or other types of vibration-isolating track designs. While the design aims of new railway projects are, typically, to keep levels of structure-borne noise in properties to below maximum levels of 40 dB(A), it has been estimated, for instance, that around 56,000 households in London are subjected to this level and a very small number experience maximum levels of above 60 dB(A).[72]

B. Surface Vibration Propagation

In a layered ground, vibration propagates parallel to the surface via a number of wave types or modes. These are often called Rayleigh waves of different order (R-waves) and Love waves. The Rayleigh waves are also called P-SV waves since they involve coupled components of compressive deformation and vertically polarised shear deformation.[b] Here, the name P-SV wave is preferred and the term Rayleigh wave is reserved for the single such wave that exists in a homogeneous half-space. Love waves are decoupled from these and only involve horizontally polarised shear deformation and so are also known as SH waves. Since the vertical forces in the track dominate the excitation of vibration in the ground the SH waves are not strongly excited. They are not considered further in the present discussion.

To illustrate, examples of the wave mode shapes of the P-SV waves are shown in Figure 10.30. These are the waves that propagate at 40 Hz in a ground modelled as a soft layer of weathered soil overlying a stiffer substratum of material. For the calculated results presented, the soft soil is a 2-m deep layer with a shear wave (S-wave) speed of 118 m/sec and dilatational wave (P-wave) speed 360 m/sec, and the substratum is a half-space with shear wave speed of 245 m/sec and dilatational wave speed of 1760 m/sec. Damping is included in both materials as a loss factor of 0.1.

If the wave number ($= 2\pi/\lambda$ with λ the wavelength) is plotted as a function of frequency, the *dispersion curve* for the wave type is generated. Figure 10.31 presents the dispersion diagram for the example soil structure (only the propagating P-SV modes are shown). Each line of the diagram represents a wave type associated with a cross-sectional mode of the layered soil. The inverse slope of a line from the origin to a point on a curve is equal to the phase velocity of that wave type at a particular frequency. The inverse slope of the curve itself gives the group velocity of the wave type. This is the speed at which energy is transported.

For this example set of soil parameters, at very low frequency, only a single mode exists and this has a wave speed close to that of the shear waves in the substratum. Around 15 Hz, the depth of the weathered material sustains a quarter wavelength of the shear wave. Above this frequency there is a "cut-on" of a wave that involves mostly deformation of the weathered layer material. With the onset of this mode, i.e., propagation via the layer material, a rise in the transmitted level of vibration is observed. It can be seen in Figure 10.30 that the mode with the lower phase speed (left-hand picture) involves mainly deformation of the softer layer material whereas the second mode involves a stronger component of deformation in the half-space.

Figure 10.31 shows that, as the frequency increases, higher order propagating wave types "cut-on" at frequencies of 23, 47, and 85 Hz. At high frequency, as the wavelengths of shear and compression become small compared with the depth of the weathered material layer, the wave number of the slowest wave converges towards that of the Rayleigh wave in a half-space of the layer material.

Figure 10.31 also presents the dispersion curve of the wave propagating along a ballasted track structure unconstrained at its lower surface (parameters as in Table 10.1). This curve is superimposed on the ground wave curves. At the intersection of the track wave curve and the first

[b] The compressive or dilatational wave is often referred to as the P-wave (P stands for primary) and the shear wave as the S-wave (S stands for secondary). In a seismic survey the faster P-wave arrives at a detector first and the S-wave second.

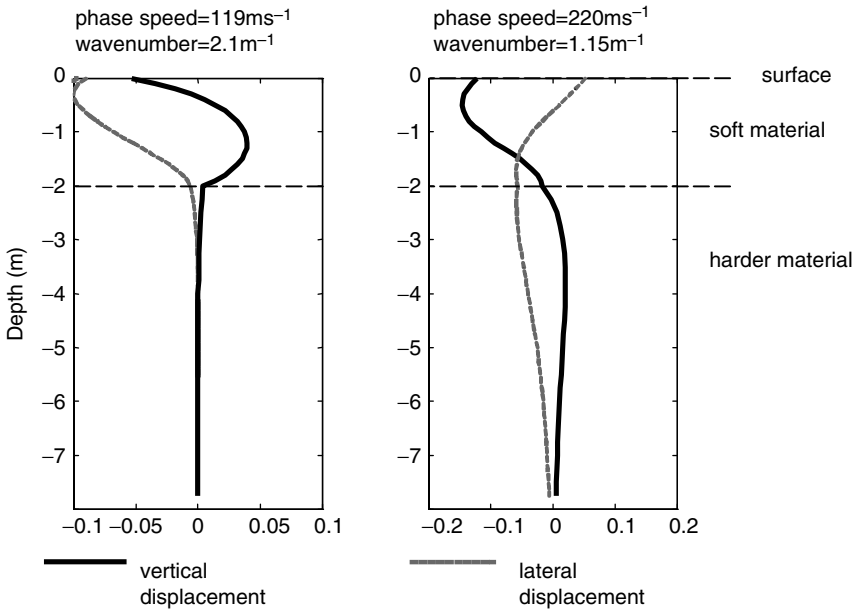

FIGURE 10.30 P-SV modes of the example layered ground structure at 40 Hz.

ground wave curve, around 35 Hz, waves may freely propagate at the same speed in both the track and the ground. The inverse of the phase speed at this intersection is represented by the slope of the straight line through this point and the origin indicated on the graph. If a moving but nonoscillating load is applied to the track at this speed, it will excite a maximum level of ground vibration. Thus the track-ground system may exhibit a critical train speed that causes high levels of vibration. If a nonoscillating load travels at a lower speed it will not directly excite propagating ground waves. The plot also shows that the response to a dynamic load not moving along the track would have a maximum at a frequency of 35 Hz. A more detailed discussion of the critical speed, and the influence of the track parameters on this, is given in Ref. 73.

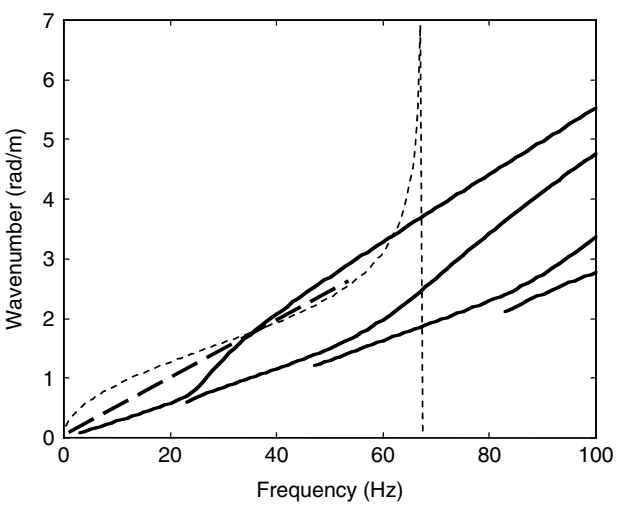

FIGURE 10.31 The dispersion diagram for propagating P-SV waves of the example ground (—), the dispersion diagram for a track (– – –), and a line representing the critical train speed (– –).

TABLE 10.1
Parameters Used for the Ballasted Track in Figure 10.31

Mass of rail beam per unit length of track	120 kg/m
Bending stiffness of rail beam	1.26×10^7 Nm^2
Loss factor of the rail	0.01
Rail pad stiffness	3.5×10^8 N/m^2
Rail pad loss factor	0.15
Mass of sleepers per unit length of track	490 kg/m
Mass of ballast per unit length of track	3300 kg/m
Ballast stiffness per unit length of track	1.775×10^8 N/m^2
Loss factor of ballast	1.0
Effective contact width of railway and ground	2.7 m

The wave field can be derived from the calculation of the excitation of waves in the ground due to excitation on the track.[74,75] The wave field for a single load moving along the track with a speed below that of any of the waves in the ground is shown in Figure 10.32. The displacement "dip" under the single load is indicated by the positive (upward) displacement under the track. Little effect is observed only a few metres away, although close to the track the passage of the quasistatic displacement pattern may be observed. Figure 10.33 shows what happens when the load travels at a speed near to the critical speed. Propagating waves may be seen travelling with significant amplitude away from the track. These exhibit the form of a "bow wave" because the load speed is greater than the speed of waves in the ground.

If vehicle models representing each of the vehicles of a train are coupled to the model for the track ground system, a theoretical model that predicts the complete vibration field can be produced.[76] A model in which the vibration excited by the moving axle loads of the whole train and that excited by the irregular vertical profile of the track for all the axles of a train has been validated by comparison with measured vibration for a number of sites.[77] Two illustrative results are presented here for vibration from an X2000 train running over very soft soil at a site called Ledsgård near Gothenburg in Sweden.

Figure 10.34 shows the measured vibration spectrum and that predicted for the whole X2000 train at 70 km/h (19.4 m/sec) for a point 7.5 m from the centre-line of the track. The measurements

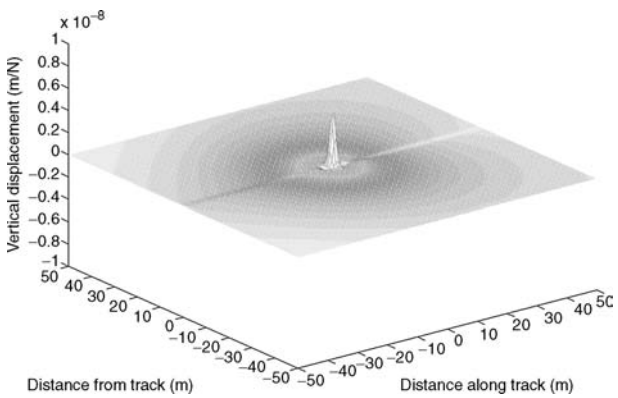

FIGURE 10.32 Displacement pattern in the moving frame of reference for a single nonoscillating axle load on the track moving at 83 m/sec, below the wavespeeds in the ground.

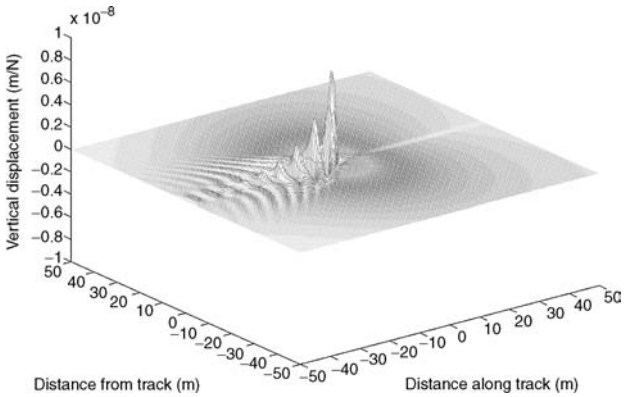

FIGURE 10.33 Displacement pattern in the moving frame of reference for a single nonoscillating axle load on the track moving at 150 m/sec, close to the critical speed for this track-ground system.

cover the frequency range from 1.6 to 40 Hz in one-third octave bands. Given that no specific track profile data were available and that therefore typical data were used, the figure shows that the predicted dynamically induced vibration level accounts well for the vibration measured over most of the frequency range. The quasistatically induced vibration is only important below 2.5 Hz.

Figure 10.35 compares predicted and measured vibration when the X2000 runs at 200 km/h (56 m/sec). In this case, the train speed is close to the critical value for this site at which wave numbers coincide approximately as illustrated, for a different ground, in Figure 10.31.

However, the coincidence of the ground wave and speed line occurs here over an extended frequency range between 3 and 10 Hz because the ground-wave dispersion curve has an almost constant slope in this range. The results show that, now, the observed level of vibration is about 35 dB higher and that it is due to the direct excitation of the propagating wave by the moving quasistatic axle loads. In summary, therefore, the effect of a ground vibration "boom" is

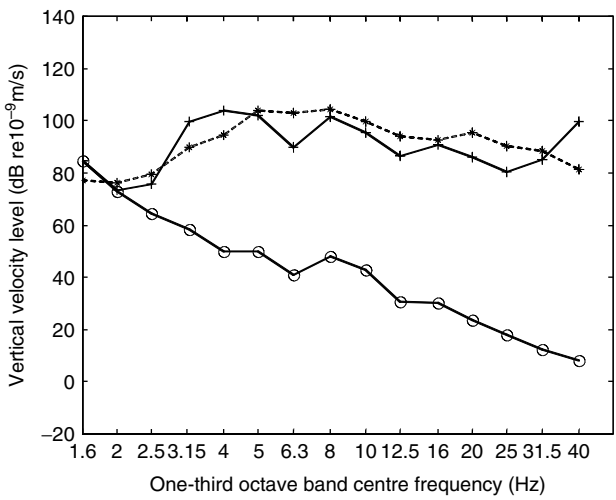

FIGURE 10.34 Vertical velocity level at Ledsgård for train speed of 70 km/h (19.4 m/sec): o predicted level due to quasistatic loads; + predicted total level; * measured level at 7.5 m. *Source*: From Sheng, X. et al., *J. Sound Vib.*, 267, 621–635, 2003, Elsevier. With permission.

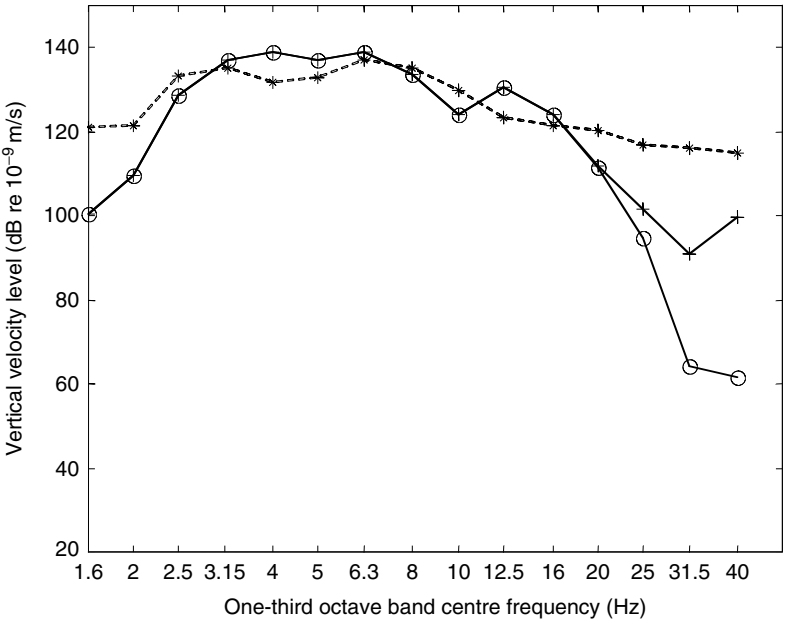

FIGURE 10.35 Vertical velocity level at Ledsgård for train speed of 200 km/h (56 m/s): o, predicted level due to quasistatic loads; +predicted total level; * measured level at 7.5 m. *Source*: From Sheng, X. et al., *J. Sound Vib.*, 267, 621–635, 2003, Elsevier. With permission.

encountered at around 200 km/h at this site, whereas at lower speed, the observed vibration level is due to the dynamically induced component of vibration.

Ledsgård is unusual in having such a low ground-wave speed and the "boom" phenomenon is therefore not common. Nevertheless, high-speed lines are now being designed for speeds in excess of 300 km/h and the critical speed must be taken into account where these pass over soft ground. For conventional trains, and for the majority of sites where vibration problems occur, however, it may be said that the most important mechanism of vibration excitation is the irregular vertical profile of the track, possibly combined with out-of-round wheels. There also remains the possibility of the succession of load-displacement dips under each axle causing vibration at the axle passing frequencies for very low frequency vibration of buildings within a few metres of the track but this does not propagate far.

C. Tunnel Vibration

Attention is now directed towards vibration propagation from tunnels. For this discussion, the results of a coupled finite element/boundary element model are presented. These are for a typical 3.5-m outer radius, circular bore tunnel (20 m deep at the rail) with and without a concrete lining.[78] Ground properties typical of a deep clay formation have been used, namely, an S-wave speed of 610 m/sec and a P-wave speed of 1500 m/sec (implying a Poisson's ratio of 0.4); the density of the material has been assumed to be 1700 kg/m^3 and the damping loss factor is 0.15. Boundary elements are used to represent the ground-tunnel interface and the ground surface from +50 to −20 m relative to the vertical centreline of the tunnel. The boundary elements model a ground of infinite extent.[78] The tunnel and invert structure are modelled using finite elements.

Figure 10.36 shows the exaggerated instantaneous particle displacement at a number of points in the ground to illustrate the wave pattern radiating away from an oscillating load at the base of the

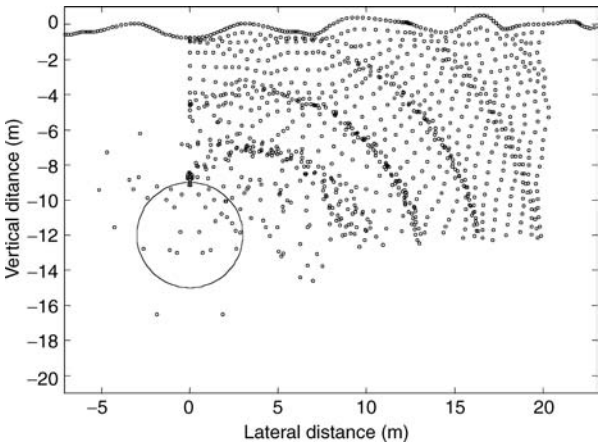

FIGURE 10.36 The vibration field around the unlined tunnel at 100 Hz. *Source*: From Jones, C. J. C., Thompson, D. J. and Petyt, M., *Transport J.*, 153(2), 121–129, 2002.

tunnel at high frequency. It shows that a relatively simple pattern of cylindrical wave fronts radiate towards the surface at greater distances from the tunnel. The strongest component of deformation in these waves is shear. At this frequency (100 Hz), the wavelengths of vibration are shorter than the diameter of the tunnel and therefore do not diffract around it. A "shadow zone" therefore exists in the region immediately above the tunnel. For this reason, the greatest amplitudes of response on the ground surface are at a distance of about 15 to 20 m from the tunnel alignment rather than directly above it.

Figure 10.37 shows the displacement of an unlined tunnel and one with a concrete lining at 100 Hz. Waves can be seen propagating from the invert slab with a high rate of decay around the ring of the unlined tunnel. These have the form of Rayleigh surface waves. Compared with the unlined tunnel, the amplitude of the response at the crown of the lined tunnel is much greater. The result is that, in the shadow zone, the tunnel structure design has a strong influence on the level of vibration at the surface.

It is clear from Figure 10.37 that the structure of the tunnel has an influence on the excitation of waves in the ground. An analysis of the waves that propagate along the tunnel structure is also possible. Figure 10.38 is similar to Figure 10.32 and Figure 10.33 in that it shows the calculated response on the surface of the ground to a moving oscillating load but, in this case, the load

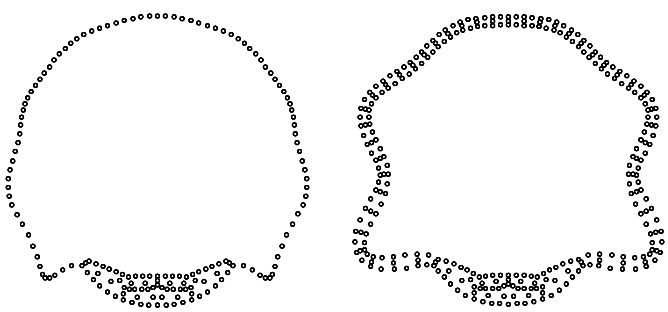

FIGURE 10.37 Amplified representation of the response showing waves round the unlined (left) and lined (right) tunnel rings at 100 Hz. *Source*: From Jones, C. J. C., Thompson, D. J. and Petyt, M., *Transport J.*, 153(2), 121–129, 2002.

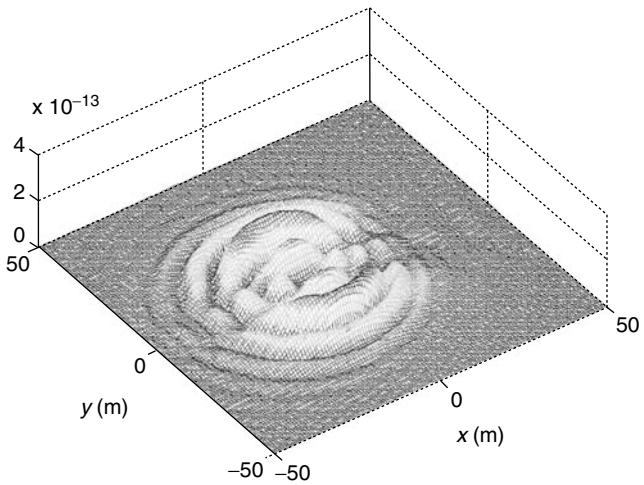

FIGURE 10.38 The vertical response amplitude of the surface of the ground to a load oscillating at 200 Hz and moving at 100 m/sec in the lined tunnel. The tunnel lies in the line $y = 0$, the invert is at a depth of 20 m.

is in a tunnel. The response can be seen to be asymmetrical because of the load speed. However, since the ground at tunnel depth is much stiffer than the soft surface conditions of Figure 10.30 to Figure 10.35, the effect of the moving load is very small even though a very high speed of 100 m/sec has been used.

As in Figure 10.36, the highest levels of vibration in Figure 10.38 can be seen to be about 15 m to the side of the centreline of the tunnel, with the propagation pattern beyond showing circular wave fronts with monotonic decay, while the vibration field above the tunnel is more complicated.

D. Vibration Isolating Tracks

The main way in which the vibration from underground railways is controlled is by the use of soft or resilient elements in the vertical support of the track in order to provide some degree of *vibration isolation*. The principle of vibration isolation is illustrated in Figure 10.39, using a simple single degree of freedom oscillator. The ratio of the amplitude of the force transmitted to the foundation to that of the oscillatory force applied to the mass is called the *transmissibility*. At very low frequency this ratio is unity; the whole force is transmitted as it would be in the static case. At the natural frequency of the system f_n, the force is increased. Above $\sqrt{2}$ times the natural frequency, the transmissibility reduces to below unity and continues to decrease with increasing frequency. The effect of the damping in the support is also shown in Figure 10.39. Here, a hysteretic damping model has been used (constant damping loss factor η) that reflects the behaviour of elastomeric materials. The amplitude of the resonance is dependent on the damping in the support but the degree of vibration isolation at higher frequencies is not.

Vibration isolating tracks are commonplace in modern underground railway systems to reduce ground-borne noise and the subject is an important part of track design. They work on a principle similar to that shown in Figure 10.39. The lower the stiffness of the support, the lower the natural frequency of the system will be and the greater the degree of vibration isolation at higher frequencies. The choice of support stiffness is, however, limited by the allowable vertical and lateral static displacements under the axle load of the train.

Figure 10.40 shows some of the basic design concepts for vibration isolating track designs. The rail pad is not shown; it has a stiffness higher than that of the resilient element in each case but possibly still significant in the behaviour of the track design for the relevant frequency range.

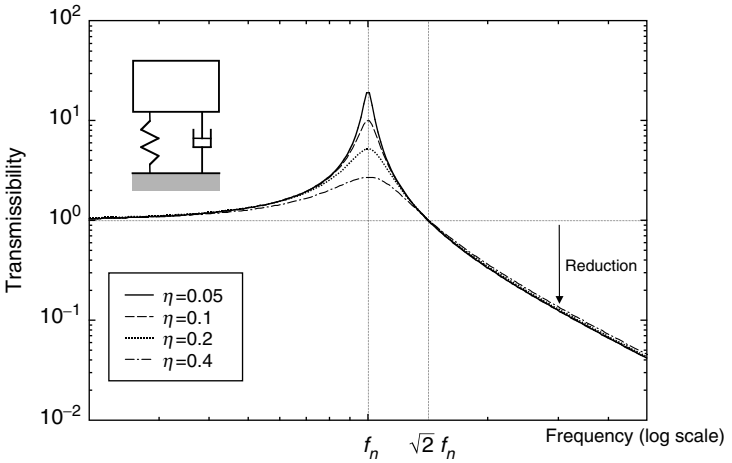

FIGURE 10.39 The force transmissibility of a hysteretically damped single degree of freedom system.

The ballast layer forms the resilient component of a conventional ballasted track. For this reason, slab tracks with normal pad stiffness give rise to increased vibration transmission compared with ballasted track. Soft baseplates are used to rectify this. For these, the lateral rail displacements are generally the limiting factor. Baseplate designs are therefore wide, or support the rail under the head, to avoid rail rotation and consequent gauge widening. Alternatively, gauge widening may be avoided by using resiliently mounted sleepers or floating slab track. These also increase the mass above the resilient element to decrease the natural frequency further.

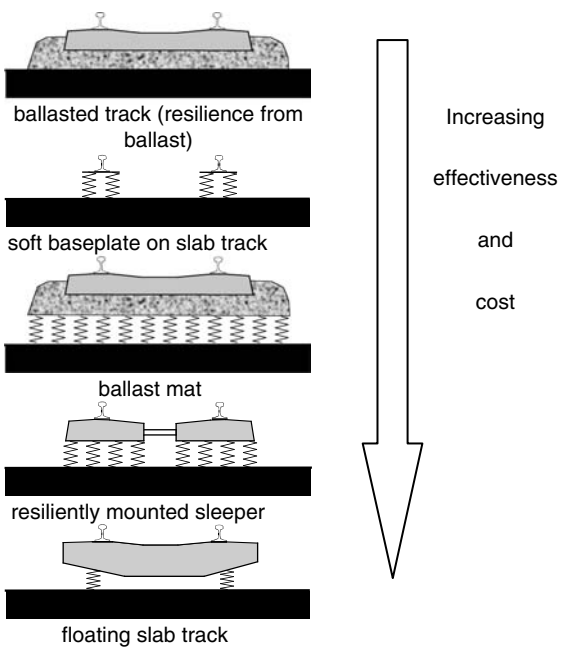

FIGURE 10.40 Design concepts for vibration isolating tracks.

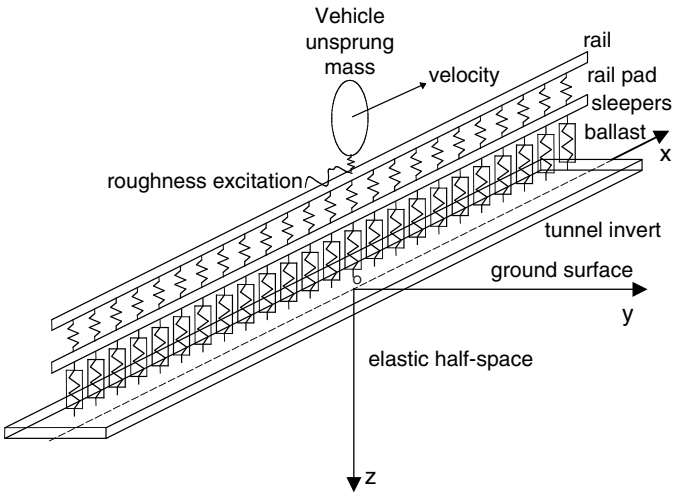

FIGURE 10.41 A model used to calculate the relative vibration isolation performance of different track designs.

Clearly, it is necessary to assess the vibration isolation performance of different track designs to obtain a required reduction in the vibration spectrum. Figure 10.41 presents a calculation model that has been extensively used for this purpose.[79] The figure shows the case for a ballasted track but different track models can be used. The model is used to predict the change in vibration response at a point of the surface of a half-space some distance from the track for a change in the parameters of the track or of the unsprung mass of the vehicle. The track is adequately modelled, for this frequency range, as an infinite layered beam structure with vertical stiffness for the ballast, pads, or baseplates distributed continuously along its length. The track-top irregularity excites a vertical dynamic force at the rail head. The model is solved in the frequency domain and hysteretic (loss factor) damping is included in all components. The elastic half-space model of the ground represents the frequency-dependent support stiffness under the track and provides a suitable means to sum the contributions of vibration from the waves propagating along the track. In this way, some geometrical and damping effects are taken into account in the propagation of vibration through the soil but the half-space does not represent a tunnel situation. The assumption is made that a vibration *reduction* due to the change in track design would be the same for a tunnel as for a half-space of realistic soil parameters. This is valid as long as the dynamic support stiffness of the ground is higher than that of the resilient element of the track.

With models similar to that shown in Figure 10.41 the performance of different track types can be evaluated for the specific vehicles and the other track parameters so that the track design can be chosen to obtain the required isolation performance at the minimum cost. The risk of the track-form leading to corrugation of the rail or high airborne noise levels in the tunnel must also be taken into account in the choice.

E. Summary

Both low frequency vibration from trains running on tracks at grade and higher frequency vibration leading to ground-borne noise in buildings are major concerns for railways. It has been shown that low-frequency surface vibration from railways may be excited either by the movement of steady axle loads or dynamically as the axles run over the irregular profile of the track. While the latter is the more dominant mechanism for conventional train speeds and frequencies above a few hertz,

the movement of the axles may be the dominant mechanism for very low frequencies at some sites close to the track. Very high levels of vibration may result from high-speed trains which can travel faster than the wave speeds in the ground at sites with very soft soil.

Ground-borne noise from trains in tunnels cannot be predicted using simple decay with distance laws, especially for locations directly over the tunnel itself. In this case the vibration response is dependent on the tunnel structure. To reduce ground-borne noise, various vibration isolating track forms are used. These should be chosen with respect to the vehicles and the vibration reduction required at particular sites.

IX. VIBRATION COMFORT ON TRAINS

A. Introduction

The level of vibration in vehicles is a major influence on the perception of the quality of rail travel in comparison with other forms of transport. Vibration in the frequency range from approximately 0.5 to 80 Hz causes discomfort as "whole body" vibration and frequencies below this may cause nausea. The wavelengths in the vertical and lateral profiles of the track that give rise to this vibration are between approximately 1 and 70 m depending on the train speed. Of course, the comfort of passengers is a primary reason for the routine monitoring and maintenance that is central to track management for all railways.

B. Assessment of Vibration Comfort in Trains

It is important to understand how measured vibration levels in vehicles are used to assess the likely reaction of passengers. A comprehensive background on this subject is given in Ref. 80; here, only an indicative overview is given.

The most commonly accepted principles of vibration perception assessment are laid out in the international standard ISO 2631-1 (1997), "Guide to the evaluation of human exposure to whole-body vibration,"[66] and also in BS 6841 (1987), "Measurement and evaluation of human exposure to whole-body mechanical vibration and repeated shock."[81] These set out terms for consideration of health, comfort, incidence of motion sickness, and effects on human activities. Frequency weightings or "filters" are defined that reflect human sensitivity to vibration in a similar way to the A-weighting (Figure 10.1) is used for sound. Some of these are shown in Figure 10.42. In the assessment of ride comfort, the filter W_b is used in BS 6841 to weight rms vibration in the vertical (spinal) direction for both seated and standing passengers and filter W_d for the two components of lateral vibration. (There is a difference between ISO 2631 and BS 6841 in that the ISO standard uses a slightly different weighting for vertical vibration, W_k. However, W_b is used more in the railway industry as is recognized in a later *draft* standard ISO 2631-4, specifically for the railway industry.) Vibration in the frequency range 0.5 to 80 Hz is considered. It is measured, as appropriate, on the seat surface between the cushion and a subject, or on the carriage floor. Since measurements on the seat are dependent on the seated person, measurements should be carried out for a sample of subjects. Vibration on the seat back can also be important and is evaluated using other frequency weightings.

When considering the effects of vibration on human activity, weighting W_g is used for the vertical direction rather than W_b. For assessing the likelihood of vibration to cause motion sickness, weighting W_f is used for vertical vibration and the lower frequency range of 0.1 to 0.5 Hz is considered. No guidance is given in the standard on the influence of other components of vibration on motion sickness.

Meters and vibration analysis equipment are available that implement the frequency weighting filters and thereby evaluate the overall weighted levels of vibration. To combine the effects of

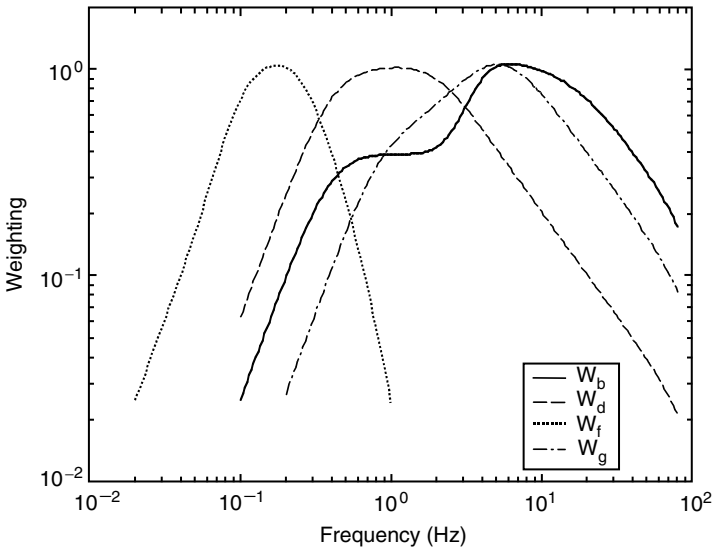

FIGURE 10.42 Some of the frequency weightings for whole body vibration defined in BS 6841.

vibration entering the body at the seat, seat back, and the floor in different directions, the root sum of squares of these overall levels can be used.

It is for the rolling stock purchaser to set acceptable limits for vibration measured in this way according to the type of rolling stock taking into account factors such as the duration of journeys, number of standing passengers, line geometry standard, vehicle speed, etc. In practice, the standards that are set vary from one railway to another.

There are a small number of single-value indicators of ride quality. One is defined by BS 6841 which allows the measurement of weighted accelerations in 12 components on the seat, seat back, and floor. These overall levels are then multiplied by "axis multiplying factors" to give "component ride values" and these may be combined to give an overall ride index.

Another ride quality indicator for "average comfort", N_{MV}, is defined by prENV 12229 (1996).[82] This uses overall accelerations in the vertical and the two horizontal component directions, weighted as in BS 6841 and ISO 2631, but the 95th percentile values of 60 separate 5-sec measurements are taken. The measure therefore becomes sensitive to rare events of high acceleration. N_{MV} is evaluated as six times the root sum of squares of these values. Values of N_{MV} are then rated in five bands from "very comfortable" ($N_{MV} < 1$) to "very uncomfortable" ($N_{MV} > 5$). Although it is suggested that all European railways should adopt this measure of "average comfort," its complexity is a barrier to its acceptance in practice.

C. Effects of Vehicle Design

Passenger vehicle suspensions are designed to isolate the coach body for frequencies above approximately 2 Hz. The bogie ride dynamics and the design of the suspension are of primary importance through much of the lower frequency range to which humans are sensitive, especially for motion sickness. In the latter case, the human effects of tilt and cant deficiency are an important ongoing area for research.

The vibration level inside the coach body is also affected by its low order structural resonances. Typically, both vertical and lateral first-order modes of bending along the coach arise at frequencies around 10 Hz and resonances of the floor occur at frequencies just above this. The excited amplitude of these should be kept to a minimum by structural design of the coach avoiding the

coincidence of important modes and using damping treatments. The coach body modes should be kept above the frequency range to which humans are most sensitive (approximately 2 to 10 Hz). This is one reason for the trend towards light, stiff materials such as aluminum extrusions in the manufacture of rolling stock.

An additional trend is the introduction of vibration-isolated "walking" floors in passenger coaches. This is primarily aimed at reducing vibration in the audible frequency range that is important for the interior noise environment (Section VII) but can be effective in reducing vibration above approximately 20 Hz.[83]

The coach body vibration, both vertical and in the two lateral directions, is felt by passengers through the seat and the seat back. Seat dynamics must also therefore be considered. The coupled system of seat and human body exhibits a resonance of vertical vibration typically between 4 and 6 Hz and at a similar frequency in fore-aft vibration due to the stiffness of the backrest. With the very soft seats used on some old rolling stock, these resonances can cause the vibration at the floor level to be made worse for the passenger, rather than better, by the seat. For this reason new rolling stock often has much firmer seats than the stock it replaces.

REFERENCES

1. Future Noise Policy, European Commission Green Paper, COM(96) 540 final, Brussels, 4 November, CB-CO-96-548-EN-C, 1996.
2. Commission Decision 2002/735/EC concerning the Technical Specification for Interoperability (TSI) relating to the rolling stock subsystem of the trans-European high-speed rail system. *Off. J. Eur. Communities* 12.9.2002 L245/402–506.
3. Fahy, F. and Walker, J., Eds., *Fundamentals of Noise and Vibration*, E&FN Spon, London, 1998.
4. Kinsler, L. E., Frey, A. R., Coppens, A., and Sanders, J. V., *Fundamentals of Acoustics*, Wiley, New York, 1982.
5. ISO 532-1975 Acoustics — method for calculating loudness level, International Organization for Standardization.
6. Dings, P. C. and Dittrich, M. G., Roughness on Dutch wheels and rails, *J. Sound Vib.*, 193, 103–112, 1996.
7. Remington, P. J., Wheel/rail noise, part IV: rolling noise, *J. Sound Vib.*, 46, 419–436, 1976.
8. Remington, P. J. and Webb, J., Estimation of wheel/rail interaction forces in the contact area due to roughness, *J. Sound Vib.*, 193, 83–102, 1996.
9. Thompson, D. J., The influence of the contact zone on the excitation of wheel/rail noise, *J. Sound Vib.*, 267, 523–535, 2003.
10. Thompson, D. J. and Jones, C. J. C., A review of the modelling of wheel/rail noise generation, *J. Sound Vib.*, 231, 519–536, 2000.
11. Wu, T. X. and Thompson, D. J., Theoretical investigation of wheel/rail non-linear interaction due to roughness excitation, *Veh. Syst. Dyn.*, 34, 261–282, 2000.
12. Thompson, D. J., Hemsworth, B., and Vincent, N., Experimental validation of the TWINS prediction program for rolling noise, part 1: description of the model and method, *J. Sound Vib.*, 193, 123–135, 1996.
13. Thompson, D. J., Fodiman, P., and Mahé, H., Experimental validation of the TWINS prediction program for rolling noise, part 2: results, *J. Sound Vib.*, 193, 137–147, 1996.
14. Jones, C. J. C. and Thompson, D. J., Extended validation of a theoretical model for railway rolling noise using novel wheel and track designs, *J. Sound Vib.*, 267, 509–522, 2003.
15. Hübner, P., The action programme of UIC, CER, and UIP 'abatement of railway noise emissions on goods trains', *J. Sound Vib.*, 231, 511–517, 2000.
16. Hölzl, G., A quiet railway by noise optimised wheels (in German), *ZEV + DET Glas. Ann.*, 188, 20–23, 1994.
17. Färm, J., Evaluation of wheel dampers on an intercity train, *J. Sound Vib.*, 267, 739–747, 2003.

18. Jones, C. J. C. and Thompson, D. J., Rolling noise generated by wheels with visco-elastic layers, *J. Sound Vib.*, 231, 779–790, 2000.
19. Cervello, S., Donzella, G., Pola, A., and Scepi, M., Analysis and design of a low-noise railway wheel, *Proc. Inst. Mech. Eng., J. Rail Rapid Transit*, 215F, 179–192, 2001.
20. Thompson, D. J. and Jones, C. J. C., A study of the use of vehicles with small wheels for determining the component of noise from the track, Proceedings of IOA Spring Conference, Salford, England, 2002.
21. Thompson, D. J., Wheel/rail noise generation, part II: wheel vibration, *J. Sound Vib.*, 161, 401–419, 1993.
22. Jones, C. J. C. and Edwards, J. W., Developing and testing of wheels and track components for reduced rolling noise from freight trains, Proceedings of Internoise '96, pp. 403–408, Liverpool, 1996.
23. Jones, C. J. C., Thompson, D. J., Frid, A., and Wallentin, M. O., *Design of a Railway Wheel with Acoustically Improved Cross-Section and Constrained Layer Damping*, Internoise 2000, Nice, France, August, pp. 673–678, 2000.
24. Vincent, N., Bouvet, P., Thompson, D. J., and Gautier, P. E., Theoretical optimization of track components to reduce rolling noise, *J. Sound Vib.*, 193, 161–171, 1996.
25. Thompson, D. J., Jones, C. J. C., and Farrington, D., *The Development of a Rail Damping Device for Reducing Noise from Railway Track*, *Internoise 2000*, Nice, France, August, pp. 685–690, 2000.
26. Jones, R. R. K., Bogie shrouds and low barriers could significantly reduce wheel/rail noise, *Rail. Gaz. Int.*, July, 459–462, 1994.
27. Jones, R., Beier, M., Diehl, R. J., Jones, C., Maderboeck, M., Middleton, C., and Verheij, J., *Vehicle-Mounted Shields and Low Trackside Barriers for Railway Noise Control in a European Context*, *Internoise 2000,* Nice, France, August, 2000.
28. Oertli, J., The STAIRRS project, work package 1: a cost-effectiveness analysis of railway noise reduction on a European scale, *J. Sound Vib.*, 267, 431–437, 2003.
29. Vér, I. L., Ventres, C. S., and Myles, M. M., Wheel/rail noise, part II: impact noise generation by wheel and rail discontinuities, *J. Sound Vib.*, 46, 395–417, 1976.
30. Clark, R. A., Dean, P. A., Elkins, J. A., and Newton, S. G., An investigation into the dynamic effects of railway vehicles running on corrugated rails, *J. Mech. Eng. Sci.*, 24, 65–76, 1982.
31. Nielsen, J. C. O. and Igeland, A., Vertical dynamic interaction between train and track — influence of wheel and track imperfections, *J. Sound Vib.*, 187, 825–839, 1995.
32. Wu, T. X. and Thompson, D. J., A hybrid model for the noise generation due to railway wheel flats, *J. Sound Vib.*, 251, 115–139, 2002.
33. Johansson, A. and Nielsen, J., *Railway Wheel Out-of-Roundness — Influence on Wheel–Rail Contact Forces and Track Response*, *Proceedings of Wheelset Congress,* Rome, 2001.
34. Wu, T. X. and Thompson, D. J., On the impact noise generation due to a wheel passing over rail joints, *J. Sound Vib.*, 267, 485–496, 2003.
35. Wu, T. X. and Thompson, D. J., *A Model for Impact Forces and Noise Generation Due to Wheel and Rail Discontinuities*, *Eighth International Congress Sound and Vibration,* Hong Kong, China, pp. 2905–2912, 2001.
36. Remington, P. J., Wheel/rail squeal and impact noise: what do we know? What don't we know? Where do we go from here?, *J. Sound Vib.*, 116, 339–353, 1987.
37. Rudd, M. J., Wheel/rail noise — part II: wheel squeal, *J. Sound Vib.*, 46, 381–394, 1976.
38. Fingberg, U., A model of wheel–rail squealing noise, *J. Sound Vib.*, 143, 365–377, 1990.
39. Périard, F., Wheel–rail noise generation: curve squealing by trams. Ph.D. thesis, Technische Universiteit Delft, 1998.
40. Heckl, M. A., Curve squeal of train wheels, part 2: which wheel modes are prone to squeal?, *J. Sound Vib.*, 229, 695–707, 2000.
41. De Beer, F. G., Janssens, M. H. A., and Kooijman, P. P., Squeal of rail bound vehicles influenced by lateral contact position, *J. Sound Vib.*, 267, 497–507, 2003.
42. Monk-Steel, A. and Thompson, D., *Models for Railway Curve Squeal Noise*, *Seventh International Conference of Recent Advances in Structural Dynamics,* Southampton, England, July, 2003.

43. Eadie, D. T., Santoro, M., and Powell, W., Local control of noise and vibration with Keltrack friction modifier and Protector trackside application: an integrated solution, *J. Sound Vib.*, 267, 761–772, 2003.
44. Wetta, P. and Demilly, F., Reduction of wheel squeal noise generated on curves or during braking, *11th International of Wheelset Congress*, Paris, June, pp. 301–306, 1995.
45. Kirschner, F., Koch, J. E., and Cohen, H. C., *Light Weight Vibration Damping Treatments for Railroad Wheels*, *11th International of Congress Acoustics,* Paris, 5, 129–132, 1983.
46. Mauclaire, B., *Noise Generated by High Speed Trains. New Information Acquired by SNCF in the Field of Acoustics Owing to the High Speed Test Programme*, *Internoise 1990,* Gothenburg, pp. 371–374, 1990.
47. King, W. F. III, A precis of developments in the aeroacoustics of fast trains, *J. Sound Vib.*, 193, 349–358, 1996.
48. Barsikow, B., Experiences with various configurations of microphone arrays used to locate sound sources on railway trains operated by DB-AG, *J. Sound Vib.*, 193, 283–293, 1996.
49. Talotte, C., Aerodynamic noise, a critical survey, *J. Sound Vib.*, 231, 549–562, 2000.
50. Hardy, A. E. J. and Jones, R. R. K., Control of the noise environment for passengers in railway vehicles, *Proc. Inst. Mech. Eng.*, 203F, 79–85, 1989.
51. Eade, P. W. and Hardy, A. E. J., Railway vehicle internal noise, *J. Sound Vib.*, 51, 403–415, 1977.
52. Guccia, L., Passenger comfort, general issues. Presented at Sixth International Workshop on Railway Noise, Ile des Embiez, France, 1998.
53. Wettschureck, R. and Hauck, G., Geräusche und Erschütterungen aus dem Schienenverkehr (Noise and ground vibration from rail traffic), In *Taschenbuch der Technischen Akusti*, 2nd ed., Heckl, M. and Müller, H. A., Eds., Springer, Berlin, 1995.
54. Hardy, A. E. J., Railway passengers and noise, *Proc. Inst. Mech. Eng.*, 213F, 173–180, 1999.
55. Willenbrink, L., *Noise Inside and Outside Vehicles and from Railway Lines*, *Proceedings of Internoise 73,* Copenhagen, 1973, pp. 362–371.
56. Hardy, A. E. J., Measurement and assessment of noise within passenger trains, *J. Sound Vib.*, 231, 819–829, 2000.
57. Shaw, N.J., The prediction of railway vehicle internal noise using statistical energy analysis techniques. M.Sc. thesis, Heriot-Watt University, 1990.
58. Kohrs, T., Structural acoustic investigation of orthotropic plates, Diploma Thesis, TU Berlin, 2002.
59. Bracciala, A. and Pellegrini, C., FEM Analysis of the internal acoustics of a railway vehicle and its improvements. WCRR 97, Florence, 1997.
60. Létourneux, F., Guerrand, S., and Poisson, F., Low-frequency acoustic transmission of high-speed trains: simplified vibroacoustic model, *J. Sound Vib.*, 231, 847–851, 2000.
61. Stegeman, B., Development and validation of a vibroacoustic model of a metro rail car using Statistical Energy Analysis (SEA). M.Sc. dissertation, Chalmers University, Gothenburg, Sweden, 2002.
62. de Meester, K., Hermans, L., Wyckaert, K., and Cuny, N., *Experimental SEA on a Highspeed Train Carriage*, *Proceedings of ISMA21,* Leuven, Belgium, pp. 151–161, 1996.
63. Geissler, P. and Neumann, D., *SEA Modelling for Extruded Profiles for Railway Passenger Coaches*, *Euro Noise 98, München, Germany*, 1998, pp. 189–194.
64. Xie, G., Thompson, D. J., and Jones, C. J. C., *A Modelling Approach for Extruded Plates*, *Proceedings of 10th International Congress on Sound and Vibration,* Stockholm, 2003.
65. Backström, D., Analysis of the sound transmission loss of train partitions. M.Sc. thesis, KTH Stockholm, 2001.
66. ISO 2631. *Evaluation of human exposure to whole body vibration, part 1 general requirements*, International Standards Organisation, Geneva, 1985.
67. BS 7385. *Evaluation and measurement for vibration in buildings, part 2: guide to damage levels from ground-borne vibration*, British Standards Institution, London, 1993.
68. DIN 4150-3. *Vibration in buildings — part 3: effects on structures*, Deutches Institut für Normung e.V., Berlin, 1999, February.
69. Krylov, V. V., Generation of ground vibration by superfast trains, *Appl. Acoust.*, 44, 149–164, 1995.

70. Madshus, C. and Kaynia, A. M., High speed railway lines on soft ground: dynamic behaviour at critical train speed, *J. Sound Vib.*, 231, 689–701, 2000.
71. Sheng, X., Jones, C. J. C., and Petyt, M., Ground vibration generated by a load moving along a railway track, *J. Sound Vib.*, 228, 129–156, 1999.
72. Edwards, J. W., *Survey of Environmental Noise and Vibration from London Underground Trains*, *Proceedings of Internoise '96,* Liverpool, pp. 2029–2032, 1996.
73. Sheng, X., Jones, C. J. C., and Thompson, D. J., A theoretical study on the influence of the track on train-induced ground vibration, *J. Sound Vib.*, 272, 909–936, 2004.
74. Sheng, X., Jones, C. J. C., and Petyt, M., Ground vibration generated by a harmonic load acting on a railway track, *J. Sound Vib.*, 225, 3–28, 1999.
75. Jones, C. J. C., Sheng, X., and Petyt, M., Simulations of ground vibration from a moving harmonic load on a railway track, *J. Sound Vib.*, 231, 739–751, 2000.
76. Sheng, X., Jones, C. J. C., and Thompson, D. J., A theoretical model for ground vibration from trains generated by vertical track irregularities, *J. Sound Vib.*, 272, 937–965, 2004.
77. Sheng, X., Jones, C. J. C., and Thompson, D. J., A comparison of a theoretical model for vibration from trains with measurements, *J. Sound Vib.*, 267, 621–635, 2003.
78. Jones, C. J. C., Thompson, D. J., and Petyt, M., A model for ground vibration from railway tunnels, *Proc. Inst. Civ. Eng., Transport.*, 153, 121–129, 2002.
79. Jones, C. J. C., *Groundborne Noise from New Railway Tunnels*, *Proceedings of Internoise '96,* Liverpool, 1996, pp. 421–426.
80. Griffin, M. J., *Handbook of Human Vibration*, Academic Press, London, 1990.
81. BS 6841, *Measurement and Evaluation of Human Exposure to Whole-Body Mechanical Vibration and Repeated Shock*, 1987.
82. CEN, *Railway Applications -Ride Comfort of Passengers — Measurement and Evaluation*, prENV 12299, 1996.
83. Wollström, M., Internal noise and vibrations in railway vehicles — a pilot study. Report TRITA — FKT 1998:44 of the Railway Technology Group, Department of Vehicle Engineering, Royal Institute of Technology (KTH), Stockholm, 1988.